Quantitative proteomics identifies novel PIAS1 substrates involved in cell migration and motility

Chongyang Li[1,2], Francis P. McManus[1], Cédric Plutoni[1], Cristina Mirela Pascariu[1], Trent Nelson[1,2], Lara Elis Alberici Delsin[1,3], Gregory Emery[1,3], Pierre Thibault [1,2,4,5*]

[1]Institute for Research in Immunology and Cancer, [2]Department of Molecular Biology, [3]Department of Pathology and Cell Biology, [4]Department of Chemistry, [5]Department of Biochemistry, Université de Montréal, Québec, Canada

***Correspondence:**
Pierre Thibault, Phone: (514) 343 6910, E-mail: pierre.thibault@umontreal.ca

Running title: Quantitative proteomics identifies novel PIAS1 substrates

Key words: SUMOylation, PIAS1, Vimentin, cell invasion, quantitative proteomics

Abbreviations:
SIM, SUMO-interacting motif; Ni-NTA, nickel-nitrilotriacetic acid; SCX, strong cation exchange; TCE, total cell extract; DMP, dimethyl pimelimidate; TFA, trifluoroacetic acid; ACN, acetonitrile; SUMO, small ubiquitin-related modifier; PML, Promyelocytic leukemia protein; PTM, post-translational modification; LC-MS/MS, liquid chromatography-tandem mass spectrometry; FDR, false discovery rate; PIAS1, Protein Inhibitor of Activated STAT, 1; SENPs, SUMO specific proteases; VIM, Vimentin; ULF, Unit-length filament; VIFs, Vimentin Intermediate Filaments;

ABSTRACT

The Protein Inhibitor of Activated STAT 1 (PIAS1) is an E3 SUMO ligase that plays important roles in various cellular pathways, including STAT signaling, p53 pathway, and the steroid hormone signaling pathway. PIAS1 can SUMOylate PML (at Lys-65 and Lys-160) and PML-RARα promoting their ubiquitin-mediated degradation. Increasing evidence shows that PIAS1 is overexpressed in various human malignancies, including prostate and lung cancers. To understand the mechanism of action of PIAS1, we developed a quantitative SUMO proteomic approach to identify potential substrates of PIAS1 in a system-wide manner. Our analyses enabled the profiling of 983 SUMO sites on 544 proteins, of which 204 SUMO sites on 123 proteins were identified as putative PIAS1 substrates. These substrates are involved in different cellular processes, such as transcriptional regulation, DNA binding and cytoskeleton dynamics. Further functional studies on Vimentin (VIM), a type III intermediate filament protein involved in cytoskeleton organization and cell motility, revealed that PIAS1 exerts its effects on cell migration and cell invasion through the SUMOylation of VIM at Lys-439 and Lys-445 residues. VIM SUMOylation was necessary for its dynamic disassembly, and cells expressing a non-SUMOylatable VIM mutant showed reduced levels of proliferation and migration. Our approach not only provides a novel strategy for the identification of E3 SUMO ligase substrates, but also yields valuable biological insights into the unsuspected role of PIAS1 and VIM SUMOylation on cell motility.

48 **INTRODUCTION**

49 The small ubiquitin-like modifier (SUMO) protein is an ubiquitin-like (UBL) protein that is
50 highly dynamic and can reversibly target lysine residues on a wide range of proteins involved in
51 several essential cellular events, including protein translocation and degradation, mitotic
52 chromosome segregation, DNA damage response, cell cycle progression, cell differentiation and
53 apoptosis[1]. SUMO proteins are highly conserved through evolution, and the human genome
54 encodes 4 SUMO genes, of which 3 genes (SUMO-1, SUMO-2 and SUMO-3) are ubiquitously
55 expressed in all cells[1,2]. Prior to conjugation, the immature SUMO proteins are C-terminally
56 processed by sentrin-specific proteases (SENPs) [3]. These proteases also cleave the isopeptide
57 bond formed between the ε-amino group of the acceptor lysine residues and the C-terminus
58 residue of the conjugated SUMO proteins. The conjugation of SUMO to target proteins requires
59 an E1 activating enzyme (SAE1/2), an E2 conjugating enzyme (UBC9) and one of several E3 SUMO
60 ligases[4]. Unlike ubiquitination, *in vitro* SUMOylation can occur without E3 SUMO ligases, although
61 enhanced substrate specificity is conferred by E3 SUMO ligases [5]. It is believed that SUMOylation
62 events occurring without the aid of E3 SUMO ligases arise primarily on the consensus motif
63 composed of ψKxE, where ψ represents a large hydrophobic residue and x, any amino acid[6]. To
64 date, several structurally unrelated classes of proteins appear to act as E3 SUMO ligases in
65 mammalian cells, such as the protein inhibitor of activated STAT (PIAS) family of proteins, Ran-
66 binding protein 2 (RanBP2), the polycomb group protein (Pc2), and topoisomerase I- and p53-
67 binding protein (TOPORS)[7,8].

68 PIAS orthologs can be found through eukaryote cells, and comprise four PIAS proteins (PIAS1,
69 PIASx (PIAS2), PIAS3, and PIASy (PIAS4)) that share a high degree of sequence homology[9]. Overall,
70 five different domains or motifs on PIAS family proteins recognize distinct sequences or
71 conformations on target proteins, unique DNA structures, or specific "bridging" molecules to
72 mediate their various functions[10]. An example of this is the PIAS Scaffold attachment factor (SAP)
73 domain which has a strong affinity towards A–T rich DNA[11] and binds to Matrix attachment
74 regions DNA[12], in addition to having an important role in substrate recognition[13]. The PINIT motif
75 affects subcellular localization and contributes to substrate selectivity[14,15]. The Siz/PIAS RING (SP-
76 RING) domain interacts with UBC9 and facilitates the transfer of SUMO to the substrate[16]. The

77 PIAS SIM (SUMO interaction motif) recognizes SUMO moieties of modified substrates and alters
78 subnuclear targeting and/or assembly of transcription complex[16-18]. While several functions have
79 been attributed to these domains, relatively little is known about the role of the poorly conserved
80 C-terminus serine/threonine-rich region.

81 PIAS1 is one of the most well studied E3 SUMO ligases, and was initially reported as the
82 inhibitor of signal transducers and activators of transcription 1 (STAT1)[19]. Previous studies
83 indicated that PIAS1 interacts with activated STAT1 and suppresses its binding to DNA [8]. PIAS1
84 overexpression was reported in several cancers, including prostate cancer, multiple myeloma,
85 and B cell lymphomas[20-23]. PIAS1 can SUMOylate the Focal adhesion kinase (FAK) at Lys-152, a
86 modification that dramatically increases its ability to autophosphorylate Thr-397, activate FAK,
87 and promotes the recruitment of several enzymes including Src family kinases[24]. In yeast, Lys-164
88 SUMOylation on Proliferating Cell Nuclear Antigen (PCNA) is strictly dependent on the PIAS1
89 ortholog Siz1, and is recruited to the anti-recombinogenic helicase Srs2 during S-phase[25]. PIAS1
90 can also regulate oncogenic signaling through the SUMOylation of promyelocytic leukemia (PML)
91 and its fusion product with the retinoic acid receptor alpha (PML-RARα) as observed in acute
92 promyelocytic leukemia (APL)[26]. In addition to its regulatory role in PML/ PML-RARα oncogenic
93 signaling, PIAS1 has been shown to be involved in the cancer therapeutic mechanism of arsenic
94 trioxide (ATO). This is accomplished by ATO promoting the hyper-SUMOylation of PML-RARα in
95 a PIAS1-dependent fashion, resulting in the ubiquitin-dependent proteasomal degradation of
96 PML-RARα and APL remission[26]. In B cell lymphoma, PIAS1 has been reported as a mediator in
97 lymphomagenesis through SUMOylation of MYC, a proto-oncogene transcription factor
98 associated with several cancers. SUMOylation of MYC leads to a longer half-life and therefore an
99 increase in oncogenic activity[23]. Altogether, these reports suggest that PIAS1 could promote
100 cancer cell growth and progression by regulating the SUMOylation level on a pool of different
101 substrates.

102 In this study, we first evaluate the effect of PIAS1 overexpression in HeLa cells. PIAS1
103 overexpression has a significant influence on cell proliferation, cell migration and cancer cell
104 invasion. To identify putative PIAS1 substrates, we developed a system level approach based on

105 quantitative SUMO proteomic analysis [27] to profile changes in protein SUMOylation in cells
106 overexpressing this E3 SUMO ligase. Our findings revealed that 204 SUMO sites on 123 proteins
107 were regulated by PIAS1. Bioinformatic analysis indicated that many PIAS1 substrates are
108 involved in transcription regulation pathways and cytoskeleton organization. Interestingly,
109 several PIAS1 substrates, including cytoskeletal proteins (Actin filaments, Intermediate filaments
110 and Microtubules), were SUMOylated at lysine residues located in non-consensus motif. We
111 confirmed the SUMOylation of several PIAS1 substrates using both *in vitro* and *in vivo*
112 SUMOylation assays. Further functional studies revealed that PIAS1 mediated the SUMOylation
113 of vimentin (VIM) at two conserved sites on its C-terminus that affect the dynamic disassembly
114 of this intermediate filament protein.

115

116 **RESULTS**

117 ***PIAS1 Overexpression Promotes cell Proliferation and Motility***

118 To investigate the physiological function of PIAS1 in HeLa cells, we overexpressed PIAS1 and
119 evaluated its expression level by western blot. The abundance of PIAS1 in HeLa cells was
120 increased by 2.5 fold at 48 h post-transfection (Fig. 1a). PIAS1 overexpression promotes HeLa cell
121 proliferation by ~50% (Fig. 1b). We further examined the phenotypic effects of PIAS1
122 overexpression on cell migration and cell invasion using wound-healing and Boyden chamber
123 invasion assays. The migration and invasion ability of Hela cells were both increased after PIAS1
124 overexpression (Figs. 1c-f). Taken together, these results highlight the role that PIAS1 plays in
125 regulating cell growth, cell cycle, cell migration and cell invasion of HeLa cells.

126

127 ***Identification of PIAS1 Regulated SUMOylation Sites by Quantitative Proteomics***

128 To gain a better understanding of the role that PIAS1 plays in cell cycle regulation, cell
129 proliferation, invasion and motility, we devised a large-scale SUMO proteomic approach to
130 identify PIAS1 substrates in a site-specific manner (Fig. 2). We combined a SUMO remnant
131 immunoaffinity strategy [27] with metabolic labeling (stable isotope labeling of amino acid in cell
132 culture, SILAC) to study the global changes in protein SUMOylation upon PIAS1 overexpression.
133 HEK293 cells stably expressing SUMO3m (Supplementary Fig. 1) were grown at 37 °C in media
134 containing light (^{0}Lys, ^{0}Arg), medium (^{4}Lys, ^{6}Arg), or heavy (^{8}Lys, ^{10}Arg) isotopic forms of lysine
135 and arginine. Three biological replicates were performed, and for each replicate, one SILAC
136 channel was transfected with an empty vector while the other two were transfected with Myc-
137 PIAS1 vectors (Fig. 2a). At 48 h post-transfection, an equal amount of cells from each SILAC
138 channel were harvested and combined before lysis in a highly denaturant buffer. PIAS1
139 overexpression efficiency in HEK293 SUMO3m cells was evaluated by western blot (Fig. 2b).
140 Protein extracts were first purified by Ni-NTA beads to enrich SUMO-modified proteins and
141 digested on beads with trypsin (Fig. 2c). Following tryptic digestion, SUMO-modified peptides
142 were immunopurified using an antibody directed against the NQTGG remnant that is revealed on

143 the SUMOylated lysine residue. Next, peptides were fractionated by offline strong cation
144 exchange (SCX) STAGE tips and analyzed by LC-MS/MS on a Tribrid Fusion instrument. To
145 determine that abundance changes were attributed to SUMOylation and not to change in protein
146 expression, we also performed quantitative proteomic analyses on the total cell extracts from
147 PIAS1 overexpression (Fig. 3a and Supplementary Fig. 2). PIAS1 overexpression caused a global
148 increase in protein SUMOylation with negligible changes on protein abundance (Fig. 3b). In total,
149 12080 peptides on 1756 proteins (Fig. 3a, Supplementary Table 1) and 983 SUMO peptides on
150 544 SUMO proteins (Fig. 3b, Supplementary Table 2) were quantified for the proteome and
151 SUMO proteome analyses, respectively. A total of 204 SUMOylation sites on 123 proteins were
152 found to be upregulated by PIAS1 overexpression including known substrates such as PCNA and
153 PML. A summary of these analyses is shown in Fig. 3 c.

154 Protein classification ontology analysis of the PIAS1 substrates using PANTHER clustered the
155 targets into 15 groups (Fig. 3d). PIAS1 mediated SUMOylation predominantly occurred on nucleic
156 acid binding proteins, transcription factors, cytoskeletal proteins, enzyme modulators, ligases
157 and chaperone proteins. We next classified putative PIAS1 substrates by their gene ontology (GO)
158 molecular function, biological process and cellular components (Fig. 3e) using the whole
159 identified SUMOylome as background. GO cellular component classification revealed that PIAS1
160 substrates were enriched in the plasma membrane and cytosol compared to the global
161 SUMOylome (Fig. 3e). This suggests that PIAS1 substrates may undergo nucleocytosolic shuttling
162 upon SUMOylation. GO biological process analysis revealed that identified PIAS1 substrates are
163 involved in a variety of biological processes, such as protein stabilization, protein folding, histone
164 H3 acetylation, translational initiation, and signal recognition particle (SRP)-dependent co-
165 translational protein targeting to membrane (Fig. 3e). GO molecular function analysis indicated
166 that PIAS1 substrates are associated with ubiquitin protein ligase binding, ubiquitin-protein
167 transferase activity and unfolded protein binding (Fig. 3e). Indeed, PIAS1 regulates the
168 SUMOylation of several proteins whose roles in the cell are diverse. Much like global
169 SUMOylation, PIAS1 mediated SUMOylation may play a role in several biological processes that
170 are independent from each other.

171 Previous SUMO proteome analyses indicated that under unstressed conditions,
172 approximately half of acceptor lysine residues are found in the SUMO consensus and reverse
173 consensus motifs[28]. Since it is believed that SUMOylation that occurs on the consensus motif
174 does not absolutely require an E3 ligase, we surmised that PIAS1 mediated SUMOylation may
175 occur at non-consensus motifs. We therefore compared the amino acid residues surrounding the
176 SUMOylation sites that are regulated by PIAS1 to those of the whole SUMO proteome
177 (Supplementary Fig. 3a). As anticipated, the sequences surrounding the PIAS1 mediated
178 SUMOylation sites are depleted in glutamic acid at position +2 and depleted of large hydrophobic
179 amino acids at position -1, consistent with the reduction of the consensus sequence. Indeed, E3
180 SUMO ligases appear to aid in the SUMOylation of lysine residues that reside in non-canonical
181 regions. Furthermore, we investigated the local secondary structures and solvent accessibility of
182 PIAS1 substrates surrounding SUMO sites using NetSurfP-1.1 software (Supplementary Fig. 3b).
183 We observed that one-third of PIAS1 regulated SUMOylation sites are located within α-helix and
184 approximately one-tenth within β-strand. In contrast, the majority of SUMOylated lysine residues
185 in the SUMO proteome are localized in coil regions. Taken together, these results support the
186 notion that PIAS1 mediated SUMOylation preferentially occurs on structured regions of the
187 protein, which may help substrate recognition by PIAS1. Additionally, we noted that PIAS1
188 mediated SUMOylation occurred primarily on solvent exposed lysine residues, which was also
189 the case for the global SUMOylome. These results suggest that PIAS1 may not impart
190 conformational changes to its substrate upon binding since it does not promote SUMOylation on
191 lysine residues that would otherwise be buried within the core of the substrate. Overall, PIAS1
192 promotes the ability of UBC9 to SUMOylate lysine residues that are present in non-consensus
193 sequences located on ordered structures of the proteins.

194 To better understand the cellular processes regulated by PIAS1, a STRING analysis was
195 performed to analyze the interaction network of putative PIAS1 substrates. This network
196 highlights the presence of highly connected interactors from promyelocytic leukemia protein
197 (PML) nuclear body, transcriptional factors, cytoskeletal proteins and RNA binding proteins (Fig.
198 4). PIAS1 was previously shown to colocalize to PML nuclear body and to regulate oncogenic

199 signaling through SUMOylation of PML and its gene translocation product PML-RARα associated
200 with acute promyelocytic leukemia (APL) [26].

201 Interestingly, we also found that several putative PIAS1 substrates were associated with
202 cytoskeletal organization including β-actin (ACTB), α-tubulin (TUBA1B), vimentin (VIM) and
203 Keratin 8 (KRT8), in addition to several other intermediate filament proteins. Of note, Keratin 8
204 was reported to be SUMOylated *in vitro* and *in vivo*, a modification that changes its dynamic
205 assembly and is increased in cells and tissues during apoptosis, oxidative stress, and phosphatase
206 inhibition[29]. The actin filaments, intermediate filaments, and microtubules that form the
207 cytoskeleton of eukaryotic cells are responsible for cell motility and division. They also help
208 establish cell polarity, which is required for cellular homeostasis and survival[30]. Moreover, one
209 SUMO site on β-actin (ACTB) and five SUMO sites on α-tubulin (TUBA1B) were found at non-
210 consensus motif regions, indicating an important role for PIAS1 in substrate protein dynamics
211 during SUMOylation. Additionally, we evaluated the degree of evolutionary conservation of these
212 modified lysine residues. Surprisingly, all SUMOylated lysine residues analyzed are highly
213 conserved across different species (Supplementary Figs. 4 and 5). In our data, we found
214 intermediate filaments (IFs) to be major targets of PIAS1 among cytoskeletal proteins. Our results
215 highlight that PIAS1 mediates the SUMOylation of the type II IF keratin 8 protein at Lys-421 and
216 the type III IF VIM protein at Lys-439 and Lys-445, both on their respective tail domains.
217 Moreover, PIAS1 promotes the SUMOylation of several type V IF proteins (e.g. Prelamin A/C,
218 Lamins B1 and B2) on their Rod domains (Supplementary Fig. 6).

219

220 ***Validation of identified PIAS1 substrates by in vitro and in vivo SUMOylation assays***

221 Next, we selected E3 SUMO-protein ligase NSE2 (NSMCE2), prefoldin subunit 2 (PFDN2) and
222 VIM, which were identified in SUMO proteomic experiments as putative PIAS1 substrates for
223 further validation. We performed both *in vitro* and *in vivo* SUMOylation assays to confirm that
224 these sites were regulated by PIAS1. For the *in vitro* SUMO assay, we incubated individual SUMO
225 substrates with SUMO-activating E1 enzyme (SAE1/SAE2), UBC9, SUMO-3 with or without PIAS1
226 in the presence of ATP. We also used PCNA, a known PIAS1 substrate, as a positive control. After

227 4h incubation at 37 °C, the western blots of each substrate showed either single or multiple bands
228 of higher molecular weight confirming the SUMOylated products. Separate LC-MS/MS
229 experiments performed on the tryptic digests of the *in vitro* reactions confirmed the
230 SUMOylation of NSMCE2 at residues Lys-90, Lys-107, and Lys-125, and PFDN2 at residues Lys-94,
231 Lys-111, Lys-132, and Lys-136. While UBC9 alone can SUMOylate these substrates, we noted an
232 increasing abundance of SUMOylated proteins when PIAS1 was present, confirming that the E3
233 SUMO ligase enhanced the efficiency of the conjugation reaction (Figure S7a). Interestingly,
234 several SUMOylation sites that were regulated by PIAS1 on both NSMCE2 and PFDN2 were not
235 located within SUMO consensus motifs, further supporting the motif analysis of the large-scale
236 proteomic data (Supplementary Fig. 3a).

237 Furthermore, we examined whether PIAS1 contributes to substrate SUMOylation *in vivo*.
238 HEK293-SUMO3 cells were co-transfected with Flag-NSMCE2, PFDN2 or VIM and Myc-PIAS1. Co-
239 transfected cells were subjected to immunoprecipitation with anti-Flag agarose gel, followed by
240 western blot with an anti-His antibody. The SUMOylation of substrates was minimally detected
241 when only transfecting Flag-substrates. In contrast, overexpression of PIAS1 under the same
242 experimental conditions led to a marked increase in the SUMOylation of these substrates
243 (Supplementary Fig. 7b). These results further confirm our quantitative SUMO proteomics data
244 and validate the proteins NSMCE2, PFDN2 and VIM as *bona fide* PIAS1 substrates.

245

246 ***PIAS1 SUMOylation Promotes its Localization to PML-NBs***

247 Interestingly, our large-scale SUMO proteomic analysis identified five SUMOylation sites on
248 PIAS1 (Fig. 5a). Two of these sites (Lys-46, Lys-56) are located in the SAP domain, and may
249 regulate the interaction of PIAS1 with DNA [15]. We also identified two SUMOylated residues (Lys-
250 137 and Lys-238) located within the PINIT domain of PIAS1, potentially affecting its subcellular
251 localization[14]. The last SUMOylated site (Lys-315) of PIAS1 and is located next to an SP-RING
252 domain, which may alter the ligation activity of PIAS1 [31]. Of note, PIAS1 contains a SUMO
253 interaction motif (SIM), and previous reports indicated that this ligase can localize to PML nuclear
254 bodies in a SIM-dependent manner with SUMOylated PML[32]. As PML also contains a SIM motif,

255 we were interested in three out of the five SUMO sites on PIAS1: Lys-137, Lys-238 and Lys-315.
256 Since PIAS1 is SUMOylated at several sites and PML contains a SIM, we surmised that reciprocal
257 interactions could be mediated through SUMO-SIM binding. Accordingly, we constructed a
258 PIAS1-GFP vector and used site-directed mutagenesis to specifically mutate the PIAS1 lysine
259 residues that are SUMO modified and are located within regions of PIAS1 that could interact with
260 PML. As the SAP domain of PIAS1 is exclusively reserved for DNA binding, we excluded the SUMO-
261 modified lysine residues in this domain when creating the mutant construct as it may affect its
262 localization in a PML independent fashion. We therefore created the variant constructs by
263 mutating the codons for Lys-K137, Lys-238 and Lys-315 to arginine codons. Several mutant genes
264 were created, including single mutants of each site, double mutant combinations, and the triple
265 mutant (PIAS1-GFP 3xKR). These mutant vectors were transfected into HEK293 SUMO3m cells
266 and used to study the effects of SUMOylation at the various lysine residues on the PIAS1-PML
267 colocalization. As evidenced by the immunofluorescence studies, approximately 45% of WT
268 PIAS1-GFP colocalized with PML (Fig. 5b). No significant changes in the colocalization of PIAS1
269 and PML were observed when experiments were repeated using either single or double PIAS1-
270 GFP mutants (data not shown). However, we noted a 50% reduction in PIAS1-GFP–PML
271 colocalization when all three sites were mutated, suggesting a possible functional redundancy
272 among these sites (Figs. 5b and 5c). The fact that the co-localization of PML and PIAS1-GFP was
273 not totally abrogated for the triple mutant might be explained by residual interactions between
274 SUMOylated PML and the SIM of PIAS1-GFP[32]. Taken together, these experiments confirmed that
275 colocalization of PIAS1 at PML nuclear bodies is partly mediated by the SUMOylation of PIAS1 at
276 Lys-137, Lys-238 and Lys-315 residues.

277

278 ***VIM SUMOylation Promotes Cell Proliferation and Motility and Increases VIF Solubility***

279 VIM is predominantly found in various mesenchymal origins and epithelial cell lines[33-35].
280 Increasing evidence shows that VIM plays key roles in cell proliferation[36], migration[37] and
281 contractility[38]. Our data shows that two SUMO sites on VIM are regulated by PIAS1, both of which
282 are located on the tail domain and are highly conserved across different species (Fig. 6a). To

283 further investigate the function of PIAS1 mediated SUMOylation of VIM, we expressed a Flag-
284 tagged VIM K439/445R double mutant (VIM^{mt}) that is refractory to SUMOylation in HeLa cells,
285 and compared the functional effects to cell expressing the wild-type Flag-tagged VIM (VIM^{wt}). We
286 transfected Flag-VIM^{wt} and Flag-VIM^{mt} into HeLa cells and used the empty Flag vector as a
287 negative control. At 48 h post-transfection, the cells were harvested, lysed in 8 M urea and
288 protein pellets were separated on SDS-PAGE. The ensuing western blot results show that protein
289 abundance between VIM^{wt} and VIM^{mt} are similar; yet, the SUMO level on VIM^{mt} is undetectable
290 (Fig. 6b). Growth assays demonstrate that VIM^{wt} expression has no effect on HeLa cell
291 proliferation while VIM^{mt} expression results in a significant inhibition of cell growth (Fig. 6c).
292 Moreover, we examined the effect of VIM^{wt} and VIM^{mt} expression on cell migration and invasion
293 using wound-healing and Boyden chamber invasion assays. VIM^{wt} significantly promotes cell
294 migration and invasion, which is in line with the results obtained in HepG2 cells[39]. However,
295 VIM^{mt} conferred no effect on cell migration or invasion (Figs. 6d-g). These results indicate that
296 SUMOylation of VIM plays a role in cell growth, migration and invasion, presumably by regulating
297 VIM IF function and/or formation.

298 Next, we investigated the function of VIM SUMOylation on the dynamics assembly of IFs. Both
299 Keratin and lamin A IFs formation and solubility have been reported to be regulated by
300 SUMOylation, while such properties have yet to be uncovered for VIM IFs[40]. For example, the
301 SUMOylation of lamin A at Lys-201, which is found in the highly conserved rod domain of the
302 protein, results in its proper nuclear localization[41]. Unlike lamin A SUMOylation, keratin
303 SUMOylation is not detected under basal conditions. However, stress-induced keratin
304 SUMOylation has been observed in mouse and human in chronic liver injuries. Additionally,
305 keratin monoSUMOylation is believed to increase its solubility, while hyperSUMOylation
306 promotes its precipitation[42].

307 We surmised that SUMOylation on VIM would alter its solubility, akin to the properties
308 observed for keratin. Accordingly, we transfected an empty vector as a negative control, VIM^{wt}
309 and VIM^{mt} into HeLa cells and lysed the cells with a RIPA buffer. Samples were fractionated into
310 RIPA soluble and insoluble fractions. Western blot analysis of these samples shows that VIM^{wt} is

311 preferentially located in the RIPA soluble fraction, while VIM^{mt} resides more in the insoluble
312 fraction (Fig. 7a). Clearly, SUMOylation of VIM drastically increases its solubility.

313 IF networks are subject to regulation by a number of phosphatases and kinases[43]. Stable VIM
314 filaments undergo extensive reorganization upon phosphorylation, a posttranslational
315 modification that controls VIM assembly and disassembly[44-46]. Multiple phosphorylation sites
316 have now been identified on VIM[47]. Those that induce disassembly are located in the N-terminal
317 head domain and are phosphorylated by multiple protein kinases. Phosphorylation of the head
318 region increases the distance between the two head groups of the VIM dimer, thus rendering the
319 VIM tetramer incapable of assembling into a filament. Activation of Akt in soft-tissue sarcoma
320 (STS) cells promotes the interaction of the head region of VIM and the tail region of Akt, resulting
321 in the phosphorylation of VIM at Ser-39, further enhancing cell motility and invasion[41].

322 Next, we sought to examine if VIM SUMOylation alters its phosphorylation status, which
323 could lead to changes in VIM IF dynamic assembly/disassembly. Accordingly, we separated
324 protein extracts from VIM^{wt} and VIM^{mt} by SDS-PAGE, excised bands that corresponded to the
325 soluble and insoluble VIM, and performed in-gel trypsin digestion followed by LC-MS/MS
326 (Supplementary Fig. 8). We identified several phosphorylated serine residues and one
327 phosphorylated threonine residue on VIM (Supplementary Table 3), which have also been
328 reported in the literature (S5, S7, T20, S22, S26, S29, S39, S42, S51, S56, S66, S72, S73, S83, S226,
329 T258 and S459). All sites except those located on the C-terminal were found to be
330 hyperphosphorylated in the insoluble VIM^{mt} compared to the wild-type counterpart.
331 Interestingly, we observed an increase phosphorylation of S39 in the insoluble pellet of VIM^{mt}, a
332 site known to be phosphorylated by Akt [41]. The observation that VIM is hyperphosphorylated at
333 its N-terminus in VIM^{mt} suggests a possible cross-talk between SUMOylation and
334 phosphorylation.

335 To further understand how SUMOylation affects VIM dynamics *in vivo*, we transfected
336 Emerald-VIM^{wt} or -VIM^{mt} vectors in VIM null MCF-7 cells. VIM null cells were employed to
337 eliminate the contribution of endogenous VIM on the VIM dynamics, which could mask the
338 phenotypic effects of our mutant. Using fluorescence microscopy we quantified the proportion

339 of the various VIM structures for the two different Emerald tagged constructs. We found three
340 major forms of VIM in the cells, which in accordance with the literature, were categorized as
341 cytosolic, unit-length filament (ULF) and VIM intermediate filaments (VIFs) (Supplementary Fig.
342 9). Statistical analysis of the proportion of the VIM structures revealed that the SUMO
343 conjugation deficient VIM (VIM^{mt}) promoted the formation of ULF with a concomitant reduction
344 in VIF formation compared to its wild-type counterpart (Fig. 7b). Taken together these results
345 indicate that SUMOylation of VIM promotes the formation of VIFs from the ULF building blocks.

346 Although VIM filament growth primarily relies on elongation by the longitudinal annealing of
347 ULFs via end-to-end fusion, recent studies suggest that the subunit exchange of tetramers within
348 these filaments does occur[48]. To determine if the SUMOylation of VIM affects the subunit
349 exchange rate of these filaments we performed fluorescence recovery after photobleaching
350 (FRAP) assays (Supplementary Fig. 10). We monitored the recovery time of filament fluorescence
351 up to 300 s after bleaching for both Emerald-VIM^{wt} and Emerald-VIM^{mt}, and noted no statistical
352 difference in recovery between constructs (Fig. 7c). This observation suggests that the
353 SUMOylation of VIM is not involved in the subunit exchange of tetramers within filaments.

354 The model described in Fig. 7d combines the results from the proteomic,
355 immunofluorescence and FRAP assays and describes the molecular mechanism of PIAS1
356 mediated control of VIM dynamics. Under physiological conditions, vimentin is maintained in
357 equilibrium between ULF and soluble tetramers. The formation of VIM ULF has been shown to
358 occur spontaneously on the order of seconds *in vitro* showing that this arrangement is
359 thermodynamically favorable and proceeds rapidly without the need for protein modifications[49].
360 Vimentin filaments elongate by end-to-end annealing of ULFs and eventually form mature
361 vimentin intermediate filaments (VIFs). This is followed by the breakdown of VIFs by severing,
362 which involves phosphorylation on several residues found on the N-term of VIM[47,50]. We show in
363 this work that this hyper-phosphorylation occurs exclusively on the N-terminal of VIM in a SUMO-
364 dependent mechanism. The truncated filaments can reanneal with another ULF to form larger
365 VIFs. However, the phosphorylated ULF must be SUMOylated by PIAS1 to increase either the
366 solubility or interaction with protein phosphatases, such as type-1 (PP1) and type-2A (PP2A)

367 protein phosphatases, as shown by the large increase in vimentin phosphorylation levels with
368 the SUMO deficient vimentin construct.[47] These results suggest that the PIAS1-mediated
369 SUMOylation of VIM stimulates the dephosphorylation of ULF and facilitate the reentry of the
370 ULF into the VIF maturation process by annealing on growing VIFs. This dynamic assembly and
371 disassembly of VIFs thus involve the SUMOylation of VIM, a modification that also regulates the
372 cell proliferation, migration and invasion (Fig. 6).

373

374 **DISCUSSION**

375 We report the functional effect of E3 SUMO ligase PIAS1 in HeLa cells, and determined that
376 PIAS1 not only promotes cell proliferation, but also stimulates cell migration and invasion. PIAS1
377 has been extensively studied in other cancer lines, such as Human Prostate Cancer, where PIAS1
378 expression is increased and enhanced proliferation through inhibition of p21[21]. In addition, other
379 studies have also reported that PIAS1 may function as a tumor suppressor to regulate gastric
380 cancer cell metastasis by targeting the MAPK signaling pathway[51]. IL-11 mediated decrease in
381 HTR-8/SVneo cells invasiveness was associated with a decrease in ERK1/2 activation, PIAS1/3-
382 mediated activated STAT3 (Tyr-705) sequestration, and a decrease in PIAS1 expression, leading
383 to a decrease in the expression of Fos and major families of metalloproteinase (MMP2, MMP3,
384 MMP9 and MMP23B)[52]. However, these studies were limited to individual PIAS1 targets to
385 understand the regulation mechanism. These targeted approaches sufficed to answer specific
386 questions about PIAS1 mediated SUMOylation, but lack the depth to fully elucidate the function
387 of PIAS1. A systematic approach to establish the global properties of PIAS1 as an E3 SUMO ligase
388 and how these SUMOylation events alter substrate function are missing and needed. Indeed,
389 such a method was never conceived due to the complex nature of quantitative SUMO
390 proteomics. Global SUMO proteome analyses are challenging due to the low abundance of
391 protein SUMOylation and the extremely large remnant that is retained on the modified lysine
392 residues upon tryptic digestion. Moreover, proteomic workflows that are currently available to
393 study SUMOylation require two levels of enrichment, which adversely affects the reproducibility
394 of SUMO site quantitation.

395 We devised an efficient method for the identification PIAS1 substrates by modifying our
396 previously described SUMO proteomics approach[27]. This method combines SILAC labelling for
397 reproducible quantitative proteomic analyses, E3 SUMO ligase protein overexpression, followed
398 by SUMO remnant immunoaffinity enrichment. This workflow allows for the selective profiling
399 of substrates and regulated SUMOylation sites of any E3 SUMO ligase. All the PIAS1 substrates
400 identified in this work were analyzed using forward and reverse SILAC labeling under basal
401 condition, which further increases the confidence of the identified substrates. Notably, we

402 observed that PIAS1 overexpression has a global effect on protein SUMOylation (Fig. 3b). This is
403 in part due to some PIAS1 substrates being directly involved in protein SUMOylation, such as
404 PIAS2, PIAS3, NSMCE2, TOPORS and TRIM28. In addition, many of the identified substrates were
405 found to participate in protein ubiquitination regulation, such as TRIM24, TRIM33, RNF2 and
406 BRCA1, which may also affect the global protein SUMOylation through the interplay between
407 SUMOylation and ubiquitination[27,53].

408 We identified five SUMOylation sites on PIAS1 itself (Lys-46, Lys-56, Lys-137, Lys-238 and Lys-
409 315), suggesting a possible feedback mechanism that could keep SUMOylation levels in check.
410 Our immunofluorescence studies show that SUMOylation of PIAS1 promotes its localization to
411 PML nuclear bodies (Figs. 5c and 5d). Interestingly, a recent paper that studied the substrates of
412 RNF4 identified PIAS1 as a substrate of this SUMO-targeted ubiquitin ligase[54]. Moreover, RNF4 is
413 localized to PML nuclear bodies, where it ubiquitylates SUMOylated proteins for their
414 subsequent proteasomal degradation. Elevated levels of cellular SUMOylation may lead to an
415 increase SUMOylation of PIAS1, prompting its localization to PML nuclear bodies and its
416 degradation by RNF4 in a ubiquitin-dependent manner. This feedback mechanism used to
417 regulate global SUMOylation may not be reserved solely for PIAS1. Indeed, other members of the
418 PIAS family, as well as NSE2 and TOPORS, have been found to be SUMOylated at several lysine
419 residues, while also being substrates of RNF4[54].

420 Notably, cytoskeletal proteins occupy a significant proportion of the identified PIAS1
421 substrates. Constituents of actin filaments, intermediate filaments and microtubules were all
422 found to be PIAS1 substrates. Interestingly, unlike UBC9 substrates that are typically SUMOylated
423 on consensus motifs[6], the acceptor lysine residues found on these cytoskeletal proteins are highly
424 conserved but are located in non-consensus sequence motif. These observations suggest that
425 PIAS1 may act as an adaptor protein to change cytoskeletal protein turnover or dynamics by
426 facilitating their SUMOylation. We uncovered that SUMOylation on the tail domain of VIM
427 increases its solubility and promotes the uptake of ULF onto VIF in a phospho-dependent
428 mechanism. The dynamic VIF disassembly/reassembly that is promoted by VIM SUMOylation in
429 turn favors cell motility and invasion, which could lead to an increase in cancer cell aggressiveness.

430 Although these findings could reveal the molecular mechanism of PIAS1 mediated VIM
431 SUMOylation and its involvement in cancer cell aggressiveness, additional evidence is required
432 to further understand the function of PIAS1-mediated SUMOylation on the other cytoskeletal
433 proteins and how these cytoskeletal proteins collaborate during cell migration.

434

435

436

METHODS

Methods and any associated references are available in the online version of the paper.

Note: Supplementary information is available in the online version of the paper

ACKNOWLEDGEMENTS

This work was funded in part by the Natural Sciences and Engineering Research Council (NSERC) (P.T., RGPIN-2018-04193) and the Canadian Institute for Health Research (CIHR) (G.E., PJT 148943, PJT 148560). C.L. was supported by a scholarship from Fonds de recherche du Québec – Nature et technologies (FRQNT). The Institute for Research in Immunology and Cancer (IRIC) receives infrastructure support from Genome Canada, the Canadian Center of Excellence in Commercialization and Research, the Canadian Foundation for Innovation, and the Fonds de recherche du Québec - Santé (FRQS).

AUTHOR CONTRIBUTIONS

C.L., F.P.M., C.P., C.M.P., T.N., L.E.A.D. performed experiments and analyzed data; C.L., F.P.M., and P.T. wrote the manuscript; G.E. and P.T. developed the concept and managed the project.

COMPETING FINANCIAL INTERESTS

The authors declare no competing financial interests.

457 **Figure Legend**

458 ***Figure 1. Functional effects of PIAS1 overexpression on HeLa cells.*** (a) HeLa cells were
459 transfected with Myc-PIAS1 or Empty vector (NC) for 48 hr. PIAS1 overexpression efficiency was
460 determined by western blot. Actin was used as a loading control. (b) PIAS1 overexpression in
461 HeLa cells significantly promotes cell growth. (c) PIAS1 overexpression increases cell migration as
462 determined by a wound-healing assay. (d) Quantification of the wound healing assay. (e)
463 Representative results from a Boyden chamber assay showing improved invasion capabilities of
464 PIAS1 overexpression in HeLa cells. (f) Quantification of the Boyden chamber assay. (*$p<0.05$,
465 **$p<0.01$, Student's t-test).

466 ***Figure 2. Workflow for the identification of PIAS1 substrates.*** (a) HEK293 SUMO3m cells were
467 cultured in SILAC medium with reverse labeling in biological triplicates. For replicate 1, PIAS1
468 overexpression was performed in medium and heavy channels with Myc-PIAS1 vector, while the
469 cells cultured in light media were transfected with the pcDNA3.0 (Empty vector). For replicates 2
470 and 3 the empty vector was transduced in the medium and heavy labelled cells, respectively. (b)
471 Western blot showing the level of overexpression of PIAS1 in the transfected cells. Detection of
472 PIAS1 overexpression by both Anti-PIAS1 antibody and Anti-Myc antibody. β-Tubulin is used as
473 loading control. (c) SILAC labelled cells were lysed and combined in a 1:1:1 ratio based on protein
474 content. SUMOylated proteins were enriched from the cell extract on an IMAC column prior to
475 their tryptic digestion. After desalting and drying, peptides containing the SUMO3 remnant were
476 enriched using a custom anti-K-ε-NQTGG antibody that was crosslinked on magnetic beads [4].
477 Enriched peptides were further fractionated on SCX columns and injected on a Tribrid Fusion
478 mass spectrometer. Peptide identification and quantification were performed using MaxQuant.

479 ***Figure 3. Statistical analyses of mass spectrometry results and bioinformatics analyses of***
480 ***identified PIAS1 substrates.*** (a) Volcano plots showing the global proteome changes in cells
481 overexpressing PIAS1 (Over.) vs. control cells (NC). Individual proteins are represented by points.
482 The area of the volcano plot where protein abundance changes are significantly regulated (p-
483 value of <0.05) are shaded in pink. (b) Volcano plots showing the global SUMOylation changes in
484 cells overexpressing PIAS1 (Over.) vs. control cells (NC). Individual SUMOylation sites are

485 represented by points. The area of the volcano plot where SUMO sites are significantly up-
486 regulated (p-value of <0.05) is shaded in pink. (c) Summary of identified and quantified peptides
487 and proteins in both the proteome and SUMOylome experiments. (d) Functional classification of
488 PIAS1 substrates using PANTHER (Protein Analysis Through Evolutionary Relationships)
489 (http://www.pantherdb.org). (e) GO term enrichment distribution of the identified PIAS1
490 substrates using DAVID 6.8 (https://david.ncifcrf.gov/).

491 ***Figure 4. Protein-Protein Interaction Network of PIAS1 substrates.*** STRING network of PIAS1
492 substrates and their interacting partners. Proteins are grouped according to their GO terms.

493 ***Figure 5. SUMOylation of PIAS1 promotes its PML localization.*** (a) Distribution of SUMO sites
494 identified on PIAS1. Three SUMO sites (K137, K237 and K315) were identified in the dataset. K137
495 and K238 are located in PINIT domain while K315 is located in SP-RING domain. (b) HEK293
496 SUMOm cells were co-transfected with PIAS1-GFP-WT or PIAS1-GFP-3xKR and
497 immunofluorescence was performed with anti-PML (scale bar, 10 µm). (c) Box plot graph showing
498 the ratio of PIAS1-PML co-localization relative to the total cell signal. (**p<0.01, Student's t-test,
499 n=10 cells/condition)

500 ***Figure 6. SUMOylation of Vimentin (VIM) is required for proper cell growth, migration and***
501 ***invasion in HeLa cells.*** (a) VIM sequence indicating SUMOylation sites at Lys 439 and Lys 445
502 localized in the tail domain, and highly conserved across six different species. (b) Western blot
503 analysis of HeLa cells transfected with an empty vector as a negative control, Wild-type vimentin
504 (Flag-VIM^{wt}), and Vimentin K439, 445R, double mutant (Flag-VIM^{mt}), showing the absence of
505 SUMOylation on the Flag-VIM^{mt} protein. (c) VIM^{mt} expression inhibits proper cell growth. (d)
506 VIM^{mt} expression inhibits proper cell migration as determined by a wound-healing assay. (e)
507 Quantification of the wound healing assay. (f) Effect of VIM^{wt} and VIM^{mt} overexpression on cell
508 invasion, as determined in a Boyden chamber assay. (g) VIM^{mt} expression significantly inhibits
509 HeLa cell invasion. (*p<0.05, **p<0.01, Student's t-test).

510 ***Figure 7. SUMOylation of Vimentin regulates its dynamic assembly.*** (a) HeLa cells were
511 transfected with an empty vector as a negative control, Flag-VIM^{wt} and Flag-VIM^{mt} and separated
512 into RIPA soluble and insoluble fractions. VIM protein levels were examined by western blot. (b)

513 MCF-7 cells were transfected with Emerald-wild-type vimentin (VIM^{wt}), and Emerald-vimentin
514 K439, 445R, double mutant (VIM^{mt}), and the proportion of unit-length filament (ULF), vimentin
515 intermediate filament (VIF) and cytosolic vimentin between VIM^{wt} and VIM^{mt} was calculated
516 under microscope (scale bar, 10 µm).(c) Fluorescence Recovery After Photobleaching (FRAP)
517 assay of Emerald-wild-type vimentin (VIM^{wt}), and Emerald-vimentin K439, 445R, double mutant
518 (VIM^{mt}) in MCF-7 cells. Line plot shows average fluorescence at each time point ± s.e.m.
519 Differences between values for VIM^{wt} and VIM^{mt} were not statistically significant at all time points
520 by Student's t-test. (d) Model of the VIM dynamic assembly and disassembly. Vimentin is
521 maintained in equilibrium between Unit-length Filament (ULF) and soluble tetramers. (Subunit
522 exchange step). Vimentin filaments elongate by end-to-end annealing of ULF to form mature
523 vimentin intermediate filament (VIF; annealing step). The phosphorylation-dependent
524 shortening of VIF (severing step) involves phosphorylation on Ser 39 and Ser 56 of vimentin by
525 several kinases, including Akt1. The short filaments can reanneal with another ULF to form new
526 VIF (re-annealing step). However, the phosphorylated ULF are not amenable to the re-annealing
527 process. These phosphorylated ULF products are subject to PIAS1-mediated SUMOylation,
528 stimulating the dephosphorylation of the phosphorylated ULF, and subsequently reenter to
529 either subunit exchange process or VIF maturation process.

530

531

532 **Figure 1:**

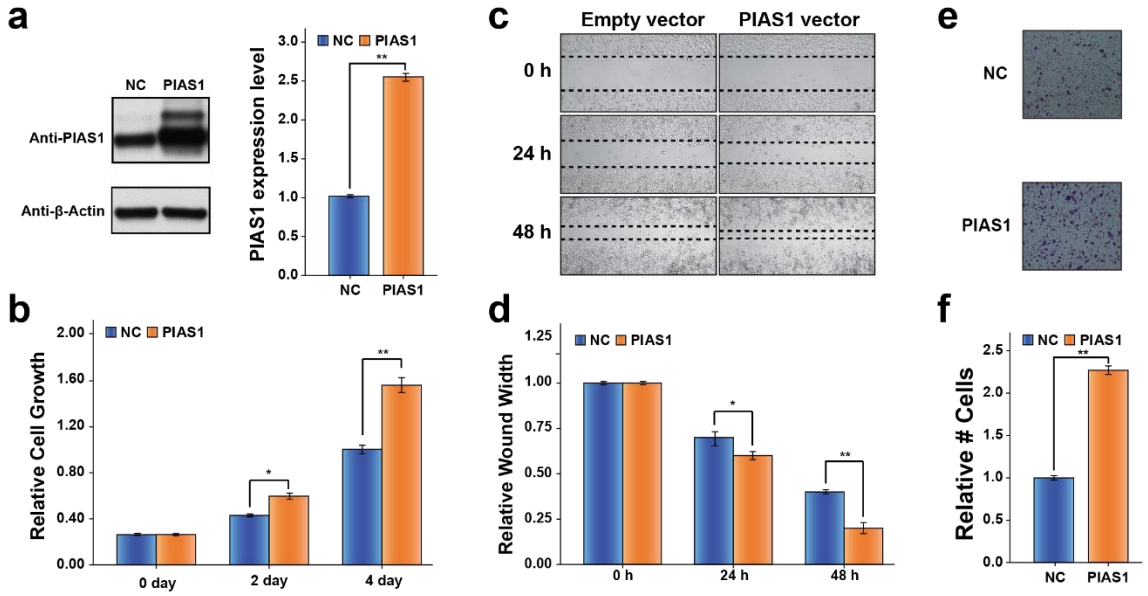

533

534 **Figure 2:**

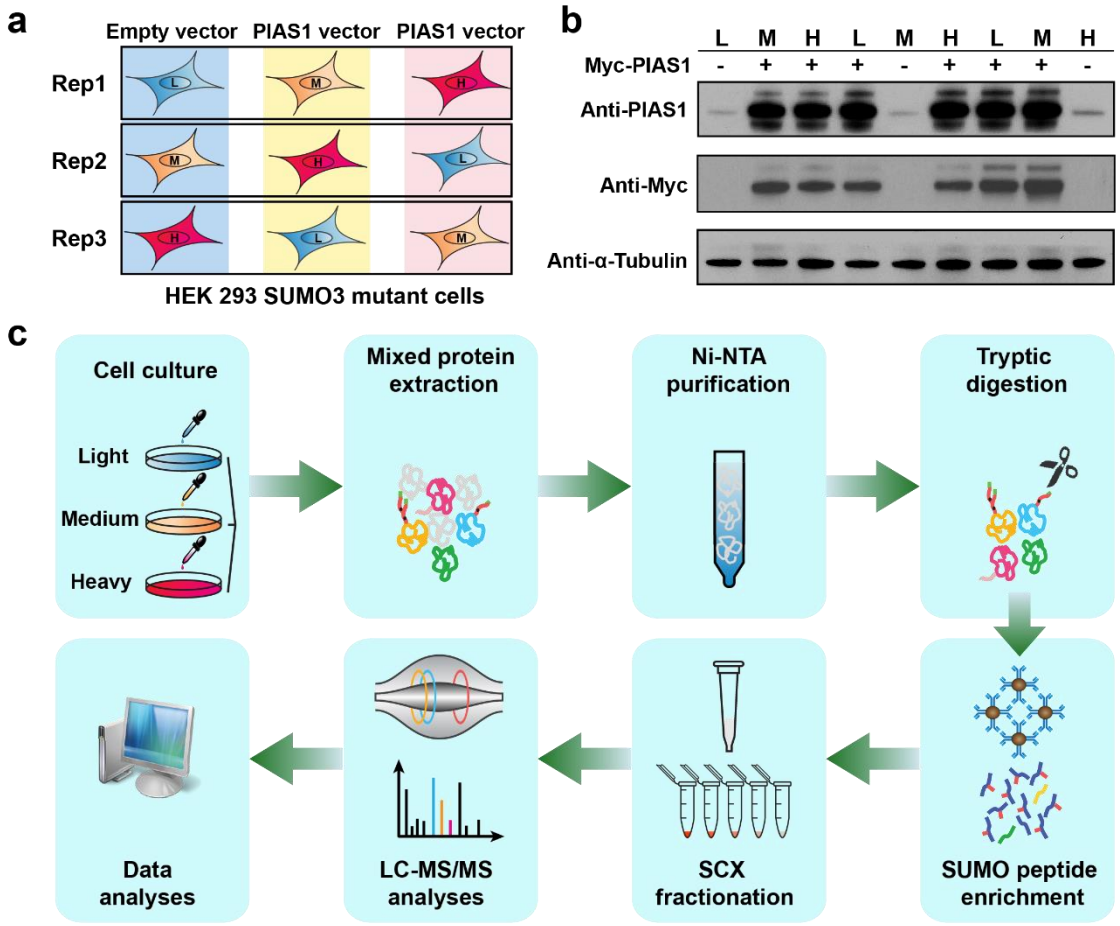

535

536

537 **Figure 3:**

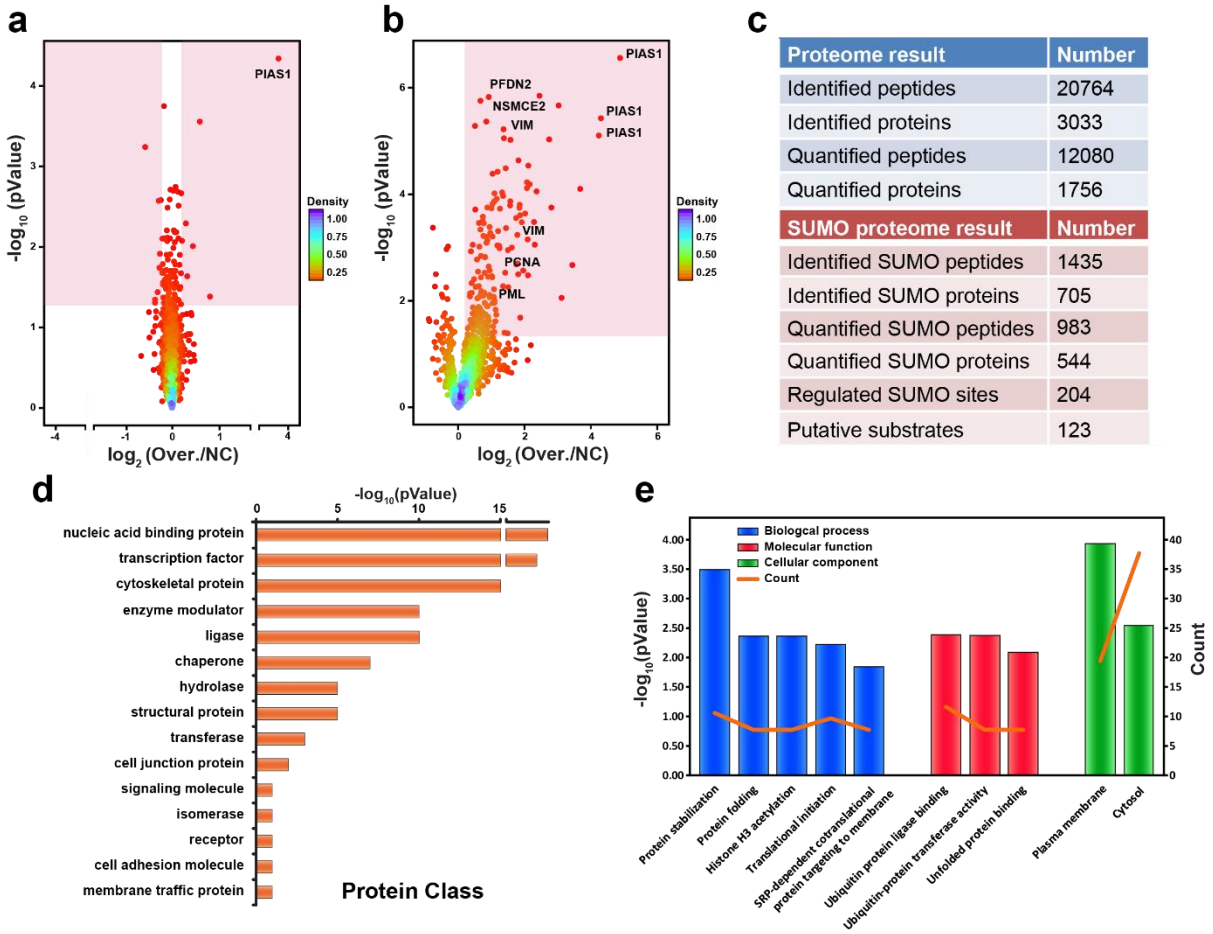

Proteome result	Number
Identified peptides	20764
Identified proteins	3033
Quantified peptides	12080
Quantified proteins	1756
SUMO proteome result	**Number**
Identified SUMO peptides	1435
Identified SUMO proteins	705
Quantified SUMO peptides	983
Quantified SUMO proteins	544
Regulated SUMO sites	204
Putative substrates	123

538

539 **Figure 4:**

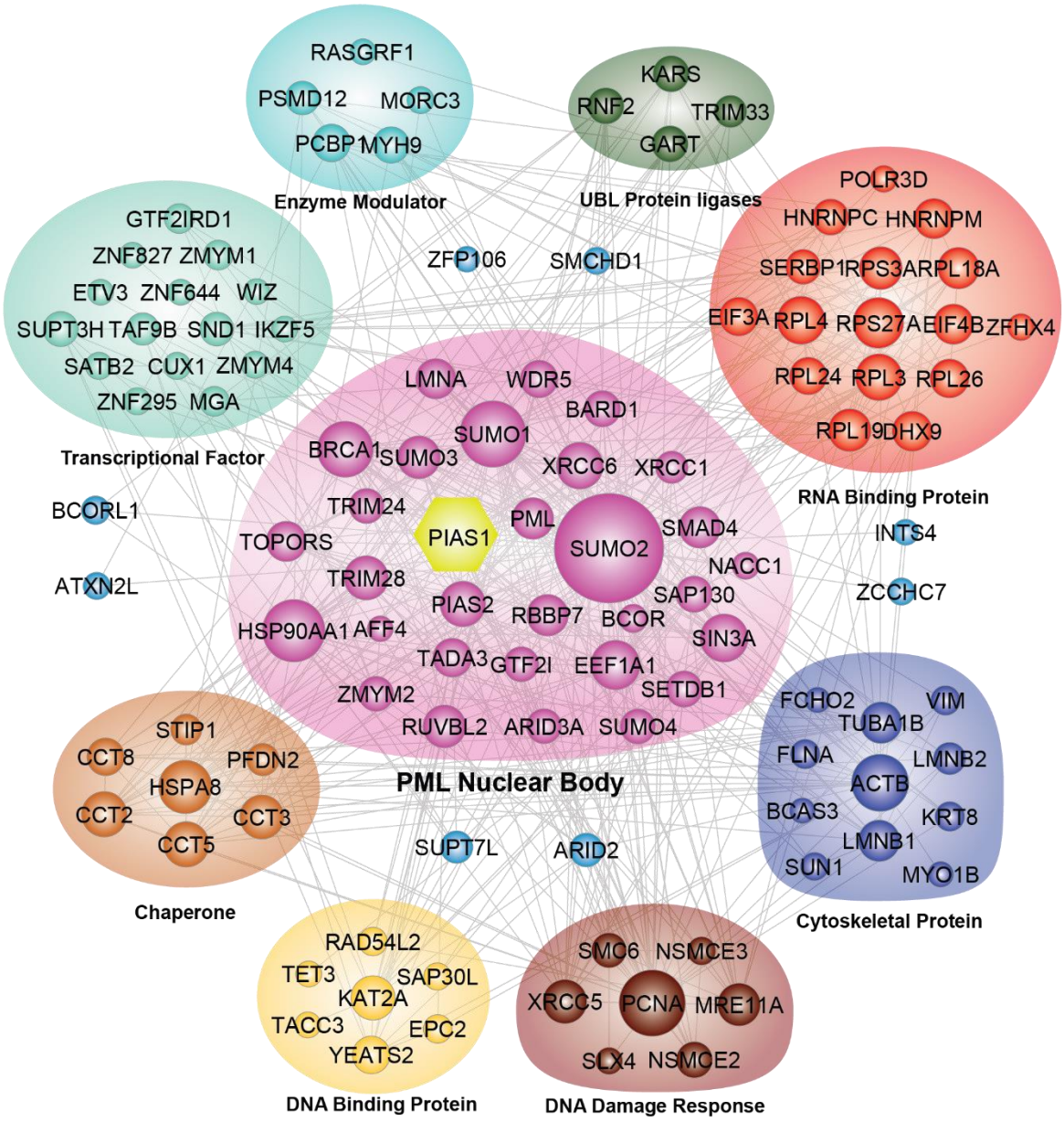

540

541 **Figure 5:**

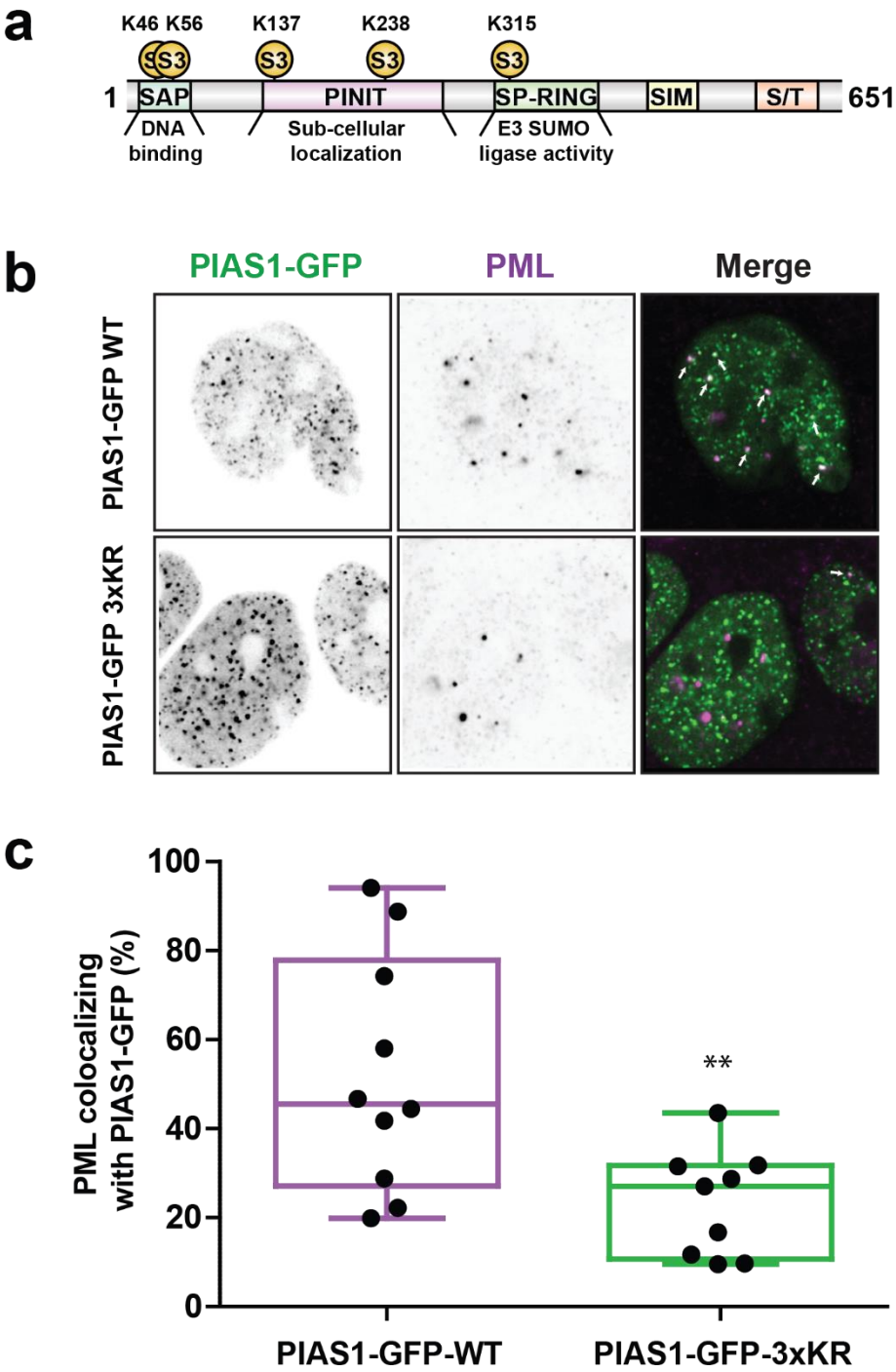

542

Figure 6:

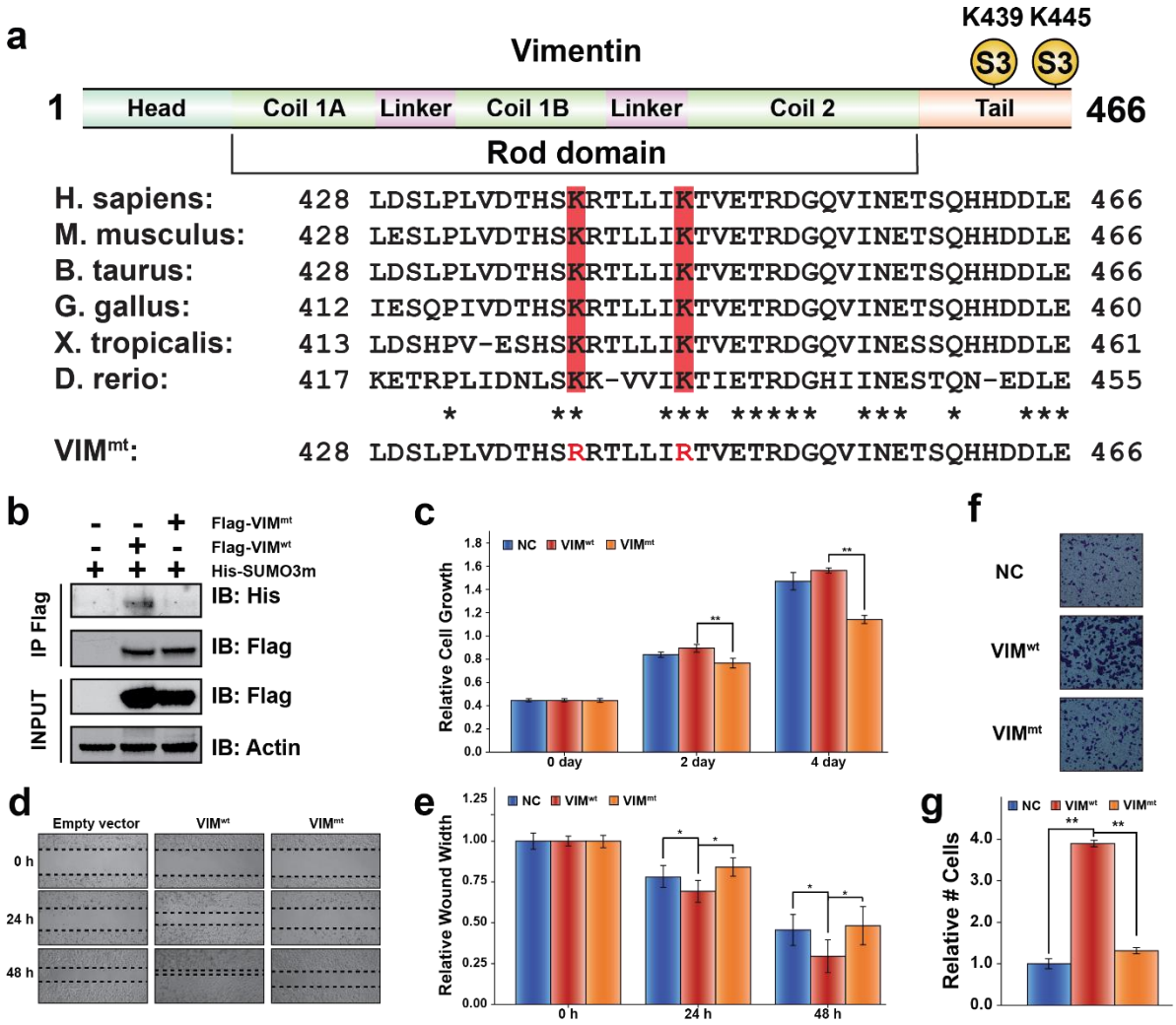
a
Vimentin
K439 K445
S3 S3
1
Head
Coil 1A
Linker
Coil 1B
Linker
Coil 2
Tail
466
Rod domain
H. sapiens: 428 LDSLPLVDTHSKRTLLIKTVETRDGQVINETSQHHDDLE 466
M. musculus: 428 LESLPLVDTHSKRTLLIKTVETRDGQVINETSQHHDDLE 466
B. taurus: 428 LDSLPLVDTHSKRTLLIKTVETRDGQVINETSQHHDDLE 466
G. gallus: 412 IESQPIVDTHSKRTLLIKTVETRDGQVINETSQHHDDLE 460
X. tropicalis: 413 LDSHPV-ESHSKRTLLIKTVETRDGQVINESSQHHDDLE 461
D. rerio: 417 KETRPLIDNLSKK-VVIKTIETRDGHIINESTQN-EDLE 455
VIMmt: 428 LDSLPLVDTHSRRTLLIRTVETRDGQVINETSQHHDDLE 466
b
Flag-VIMmt
Flag-VIMwt
His-SUMO3m
IP Flag
INPUT
IB: His
IB: Flag
IB: Flag
IB: Actin
c
NC VIMwt VIMmt
Relative Cell Growth
0 day
2 day
4 day
f
NC
VIMwt
VIMmt
d
Empty vector
VIMwt
VIMmt
0 h
24 h
48 h
e
NC VIMwt VIMmt
Relative Wound Width
0 h
24 h
48 h
g
NC VIMwt VIMmt
Relative # Cells

544

Figure 7:

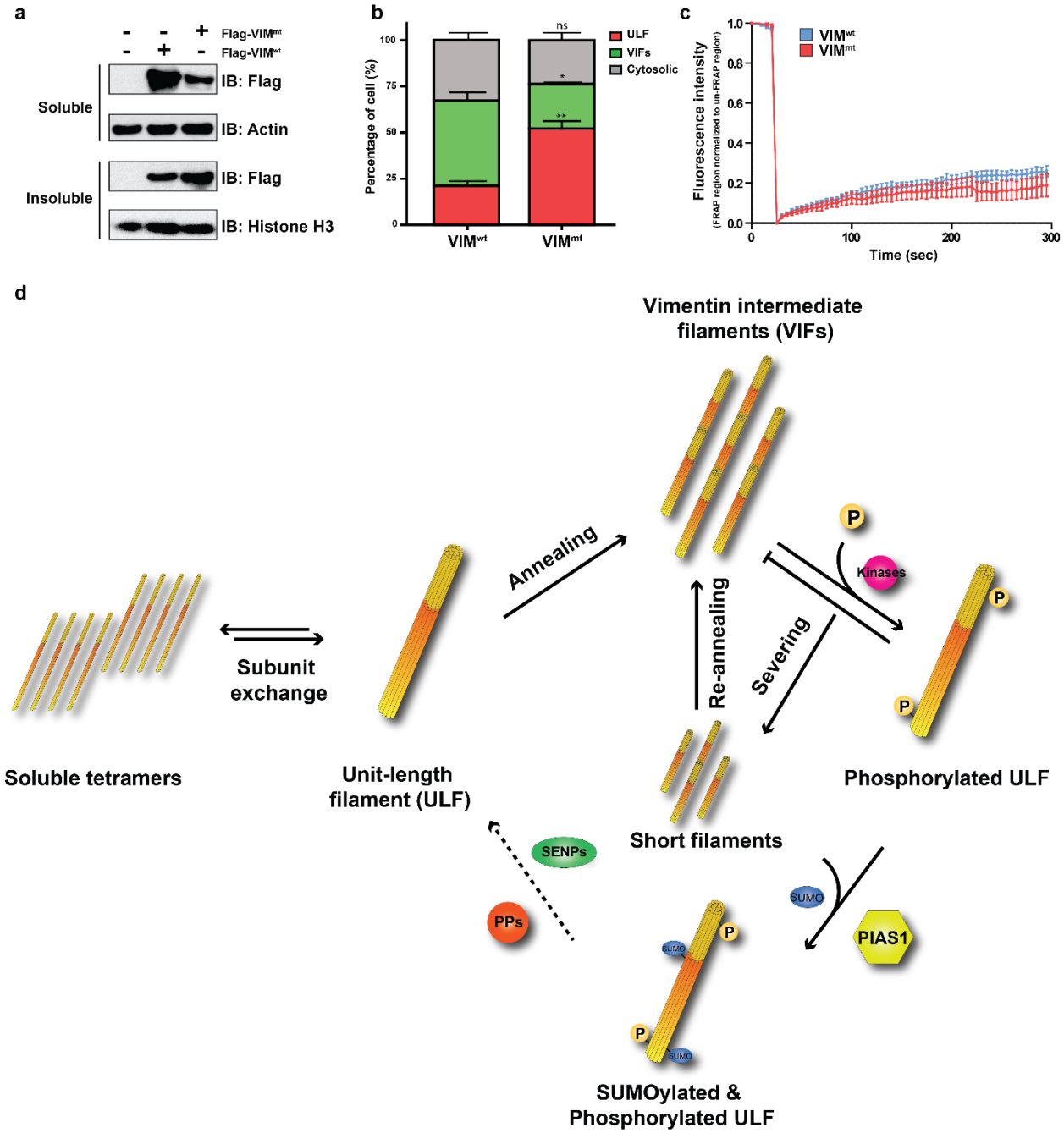
a
Flag-VIMmt
Flag-VIMwt
Soluble
IB: Flag
IB: Actin
Insoluble
IB: Flag
IB: Histone H3
b
Percentage of cell (%)
ULF
VIFs
Cytosolic
ns
VIMwt
VIMmt
c
Fluorescence intensity
(FRAP region normalized to un-FRAP region)
VIMwt
VIMmt
Time (sec)
d
Vimentin intermediate filaments (VIFs)
Annealing
Subunit exchange
Soluble tetramers
Unit-length filament (ULF)
Re-annealing
Severing
Kinases
Phosphorylated ULF
Short filaments
SENPs
PPs
SUMO
PIAS1
SUMOylated & Phosphorylated ULF

547 **METHODS**

548 Methods and any associated references are available in the online version of the paper.

549 *Note: Supplementary information is available in the online version of the paper*

550

551

552 **Online Methods**

553 ***Cell Culture and Transfection***

554 Human cervical cancer cell line (HeLa) and HEK293 stably expressing the 6xHis-SUMO3-Q87R/Q88N
555 mutant (HEK293-SUMO3m)[27] were cultured in Dulbecco's modified Eagle's medium (HyClone)
556 supplemented with 10% fetal bovine serum (Wisent), 1% L-glutamine (Thermo Fisher Scientific), 1%
557 penicillin/streptomycin (Invitrogen) in 5% CO2 at 37 °C. The mammalian expression vector for Myc-PIAS1
558 and 6xHis-SUMO3 were constructed by inserting the full-length cDNAs into pcDNA3.0-Myc and pcDNA3.0-
559 6xHis vectors, respectively. The mammalian expression vector for PIAS1-GFP-WT was constructed by
560 cloning full-length PIAS1 cDNA into pcDNA3.1-c-GFP10. The PIAS1-GFP-3xKR plasmid was generated by
561 site-directed mutagenesis using the GENEART Site-Directed Mutagenesis System according to the
562 instructions of the manufacturer (InvitrogenTM). The mammalian expression vectors pReceiver-M11
563 (Flag-NSMCE2, Flag-PFDN2 and Flag-VIM) and the bacterial expression vectors pReceiver-B11 (His-
564 NSMCE2 and His-PFDN2) were purchased from Genecopoeia, Inc. (Rockville, MD).

565 For transient transfection, HeLa cells or HEK293-SUMO3m cells were transfected with 1 μg plasmid per
566 million cells using JetPrime Reagent (Polyplus-transfection) according to the manufacturer's protocol.
567 Cells were collected 48 h after transfection and protein overexpression was confirmed by western blot.

568 ***Cell Proliferation Assay***

569 The cell proliferation assay was carried out using WST-1 Cell Proliferation Assay Kit (Roche). Transfected
570 cells were seeded into 96-well plates at a density of 1×10^3 cells/well. After 0, 2 and 4 days of incubation,
571 WST-1 reagents were added to each well, and cells were further incubated at 37 °C for 1 h. Each
572 measurement was performed in triplicate, and the experiments were repeated three times. The relative
573 numbers of viable cells were estimated using the absorbance optical density (OD) at 450 nm.

574

575 ***Migration Assays***

576 Cell migration was assessed by using a wound-healing assay. Transfected cells were seeded as a single
577 monolayer into 12-well plates at 80%-90% confluence and then scratched using a 200-µl pipette tip. After
578 the scratch, the cells were washed twice with PBS to remove the cell debris and grown in DMEM
579 containing 1% FBS. Phase-contrast microscopy images of the wound area were taken at time 0 h, 24 h and
580 48 h, wound healing was estimated by measuring the relative width.

581 ***In vitro Transwell Invasion Assays***

582 Invasive ability of transfected HeLa cells was assessed using BioCoat Matrigel Invasion Chamber (Corning)
583 which consists of a 24-well Falcon TC Companion Plate and 8 µm pore size PET membrane with a thin layer
584 of MATRIGEL Basement Membrane Matrix. Chambers were rehydrated by adding 0.5 ml DMEM
585 containing 10% FBS to the interior of the inserts and bottoms of wells. The chambers were incubated in a
586 humidified tissue culture incubator at 37°C for 2 h. After rehydration, the medium was carefully removed
587 without disturbing the layer of Matrigel. Transfected HeLa cells were seeded at 2.5 x 10^4 cells in 0.5 ml of
588 serum-free DMEM to the interior of the inserts. DMEM containing 10% FBS was added to the bottoms of
589 wells. Following a 48 h incubation at 37°C, adherent cells on the upper layer of the insert were removed
590 by gentle scraping with a cotton tip applicator. Cells that had invaded the underside of the inserts were
591 fixed with 100% methanol for 10 minutes at −20°C and stained with 0.5% crystal violet dye (EMD Millipore)
592 for 10 min at room temperature. The permeated cells were imaged under a Phase-contrast microscope.
593 Then cells were incubated with 10% acetic acid to elute the dye and the relative cell numbers were
594 estimated using the absorbance optical density (OD) at 590 nm.

595 ***SILAC Labeling and Protein Extraction***

596 HEK293-SUMO3m cells were grown in DMEM (Thermo Fisher Scientific) containing light (0Lys, 0Arg),
597 medium (4Lys, 6Arg) or heavy (8Lys, 10Arg) isotopic forms of lysine and arginine (Silantes) for at least 6
598 passages to ensure full labeling. For each triple SILAC experiment, the control channel was transfected
599 with an empty-pcDNA3.0-Myc vector while the other two channels were transfected with the Myc-PIAS1
600 plasmid. After 48 h transfection, an equal amount of cells from each SILAC channel were combined and
601 washed twice with ice-cold PBS, lysed in NiNTA denaturing incubation buffer (6 M Guanidinium HCl, 100
602 mM NaH_2PO_4, 20 mM 2-Chloroacetamide, 5 mM 2-Mercaptoethanol, 10 mM Tris-HCl pH=8) and
603 sonicated. Protein concentration was determined using micro Bradford assay (Bio-Rad).

604 ***Protein Purification, Digestion and Desalting***

605 For each replicate, 16 mg of total cell extract (TCE) were incubated with 320 µL of NiNTA beads (Qiagen)
606 at 4 °C. After 16 h incubation, NiNTA beads were washed once with 10 mL of NiNTA denaturing incubation
607 buffer, 5 times with 10 mL of NiNTA denaturing washing buffer (8 M urea, 100 mM NaH_2PO_4, 20 mM
608 imidazole, 5 mM 2-Mercaptoethanol, 20 mM Chloroacetamide, 10 mM Tris-HCl pH=6.3) and twice with
609 10 mL of 100 mM ammonium bicarbonate. Protein concentration was determined using micro Bradford
610 assay (Bio-Rad). Protein digestion on beads was carried out using a ratio 1:50 sequencing grade modified
611 trypsin (Promega): protein extract in 100 mM ammonium bicarbonate at 37 °C overnight. To quench the
612 reaction, 0.1% trifluoroacetic acid (TFA) was added. The solution was desalted on hydrophilic-lipophilic
613 balance (HLB) cartridges (1cc, 30 mg)(Waters) and eluted in LoBind tubes (Eppendorf) before being dried
614 down by Speed Vac.

615 ***SUMO Peptide Enrichment***

616 PureProteome protein A/G magnetic beads (Millipore) were equilibrated with anti-K(NQTGG) antibody at
617 a ratio of 1:2 (v/w) for 1 h at 4 °C in PBS. Saturated beads were washed 3 times with 200 mM
618 triethanolamine pH=8.3. For crosslinking, 10 µl of 5 mM DMP in 200 mM triethanolamine pH=8.3 was
619 added per µl of slurry and incubated for 1 h at room temperature. The reaction was quenched for 30
620 minutes by adding 1 M Tris-HCl pH=8 to a final concentration 5 mM. Cross-linked beads were washed 3
621 times with ice-cold PBS and once with PBS containing 50% glycerol. The tryptic digests were resuspended
622 in 500 ul PBS containing 50% glycerol and supplemented with cross-linked anti-K-(NQTGG) at a ratio of
623 1:2 (w/w). After 1 h incubation at 4 °C, anti-K-(NQTGG) antibody bound beads were washed three times
624 with 1 ml of 1 × PBS, twice with 1 ml of 0.1 × PBS and once with ddH2O. SUMO peptides were eluted three
625 times with 200 µl of 0.2% formic acid in water and dried down by Speed Vac.

626 ***SCX Fractionation***

627 Enriched SUMO peptides were reconstituted in water containing 15% acetonitrile and 0.2% formic acid
628 and loaded on conditioned strong cation exchange (SCX) StageTips (Thermo Fisher Scientific). Peptides
629 were eluted with ammonium formate pulses at 50, 75, 100, 300, 600 and 1,500 mM in 15% acetonitrile,
630 pH=3. Eluted fractions were dried down by Speed Vac and stored at −80 °C for MS analysis.

631 ***Mass Spectrometry Analysis***

632 Peptides were reconstituted in water containing 0.2% formic acid and analyzed by nanoflow-LC-MS/MS
633 using an Orbitrap Fusion Mass spectrometer (Thermo Fisher Scientific) coupled to a Proxeon Easy-nLC
634 1000. Samples were injected on a 300 µm ID × 5 mm trap and separated on a 150 µm × 20 cm nano-LC
635 column (Jupiter C18, 3 µm, 300 A, Phenomenex). The separation was performed on a linear gradient from
636 7 to 30% acetonitrile, 0.2% formic acid over 105 minutes at 600 nl/min. Full MS scans were acquired from
637 m/z 350 to m/z 1,500 at resolution 120,000 at m/z 200, with a target AGC of 1E6 and a maximum injection
638 time of 200 ms. MS/MS scans were acquired in HCD mode with a normalized collision energy of 25 and
639 resolution of 30,000 using a Top 3 s method, with a target AGC of 5E3 and a maximum injection time of
640 3,000 ms. The MS/MS triggering threshold was set at 1E5 and the dynamic exclusion of previously
641 acquired precursor was enabled for 20 s within a mass range of ±0.8 Da.

642 ***Data Processing***

643 MS data were analyzed using MaxQuant (version 1.5.3.8)[55,56]. MS/MS spectra were searched against
644 UniProt/SwissProt database (http://www.uniprot.org/) including Isoforms (released on 10 March 2015).
645 The maximum missed cleavage sites for trypsin was set to 2. Carbamidomethylation (C) was set as a fixed
646 modification and acetylation (Protein N term), oxidation (M), deamination (NQ) and NQTGG (K) were set
647 as variable modifications. The option match between runs was enabled to correlate identification and
648 quantitation results across different runs. The false discovery rate for peptide, protein, and site
649 identification was set to 1%. SUMO sites with a localization probability of >0.75 were retained. The mass
650 spectrometry proteomics data have been deposited to the ProteomeXchange Consortium
651 (http://proteomecentral.proteomexchange.org) via the PRIDE partner repository with the dataset
652 identifier <PXD011932>. Reviewer account details: Username: reviewer91455@ebi.ac.uk, Password:
653 ScCPBsuC

654 ***Bioinformatics Analysis***

655 Classification of identified PIAS1 substrates was performed using PANTHER (Protein Analysis Through
656 Evolutionary Relationships) (http://www.pantherdb.org), which classifies genes and proteins by their
657 functions[57,58]. The identified PIAS1 substrates were grouped into the biological process, molecular
658 function and cellular component classes against the background of quantified SUMOylome using DAVID
659 Bioinformatics Resources 6.7[59]. The aligned peptide sequences with ±6 amino acids sounding the modified
660 lysine residue obtained in Andromeda were submitted to IceLogo[60]. For peptide sequences corresponding

661 to multiple proteins, only the leading sequence was submitted. The secondary structures surrounding the
662 PIAS1-regulated SUMO sites were investigated using NetSurfP-1.1 (Petersen et al. 2009)[61]. INTERPRO
663 Protein Domains Analysis and Protein-Protein Interaction (PPI) network of identified PIAS1 substrates
664 were built by searching against the STRING (Search Tool for the Retrieval of Interacting Genes/Proteins)
665 database version 9.1[62,63]. All predictions were based on experimental evidence with the minimal
666 confidence score of 0.4, which is considered as the highest confidence filter in STRING. PPI networks were
667 then visualized by Cytoscape v3.5.1[64,65].

668 ***Recombinant Protein Purification and in vitro SUMO Assay***

669 The bacterial expression vectors pReceiver-B11 for His-NSMCE2 and His-PFDN2 recombinant protein
670 expression were purchased from Genecopoeia, Inc (Rockville, MD). pReceiver-B11 was individually
671 transformed into ArcticExpress Competent Cells . Transformed bacteria were cultured in LB medium until
672 an OD600 of 0.5. Isopropyl β-D-1-thiogalactopyranoside (IPTG) (Bioshop) was added to the culture at a
673 final concentration of 1 mM and the desired expression of the protein was inducted for 24h at 13°C.
674 Harvested bacterial pellets were lysed and sonicated in a solution containing 500 mM NaCl, 5 mM
675 imidazole, 5 mM β-Mercaptoethanol, 50 mM Tris-HCl pH=7.5. His-tagged proteins were purified on NiNTA
676 beads (Qiagen). Purified proteins were eluted with 500 mM NaCl, 250 mM imidazole, 5 mM β-
677 mercaptoethanol , 50 mM Tris-HCl pH=7.5 and concentrated on 3 kDa Ultra centrifugal filters (Amicon).
678 Recombinant human PCNA protein was a generous gift from Dr. Alain Verreault (University of Montreal,
679 Canada). The *in vitro* SUMO assay was carried out in a buffer containing 5 mM $MgCl_2$, 5 mM ATP, 50 mM
680 Tris-HCl pH=7.5. The enzymes responsible for the SUMOylation reaction were added at the following
681 concentrations: 0.1 µM SAE1/2, 1 µM Ubc9, 10 µM SUMO-3 and 60 nM PIAS1. The reactions were
682 incubated at 37 °C for 4 h and analyzed by western blot using an anti-His antibody.

683 ***In vivo SUMO Assay and Immunoprecipitation***

684 HEK293-SUMO3m cells were co-transfected with Myc-PIAS1, Flag-NSMCE2, Flag-PFDN2 or Flag-VIM. At
685 48 h post-transfection, cells were harvested and lysed with 1 ml of Triton lysis buffer (150 mM NaCl, 0.2%
686 Triton X-100, 1 mM EDTA, 10% Glycerol, 50 mM Tris-HCl pH 7.5) supplemented with protease inhibitor
687 cocktail (Sigma Aldrich) at 4 °C for 15 min with gentle rocking. TCE were incubated with anti-Flag M2
688 Affinity Agarose Gel (Sigma Aldrich) with gentle rocking at 4 °C for overnight. Immunoprecipitates were
689 then washed three times with cold Triton lysis buffer and were analyzed by western blot using an anti-His
690 antibody (Sigma Aldrich).

691

692 ***Western Blot***

693 TCE prepared in Triton lysis buffer were diluted in Laemmli buffer (10% (w/v) glycerol, 2% SDS, 10% (v/v)
694 2-mercaptoethanol and 62.5 mM Tris-HCl, pH=6.8), boiled for 10 min and separated on a 4–12% SDS-
695 PAGE (Bio-rad) followed by transfer onto nitrocellulose membranes. Before blocking the membrane for 1
696 h with 5% non-fat milk in TBST (Tris-buffered saline with Tween 20), membranes were briefly stained with
697 0.1% Ponceau-S in 5% acetic acid to represent total protein content. Membranes were subsequently
698 incubated overnight with a 1:1000 dilution of antibodies at 4 °C. Membranes were then incubated with
699 peroxidase-conjugated anti-mouse or anti-rabbit IgG (Cell Signaling Technology) for 1 h at room
700 temperature at a 1:5000 dilution. Membranes were washed three times with TBST for 10 minutes each
701 and revealed using ECL (GE Healthcare) as per the manufacturer's instructions. Chemiluminescence was
702 captured on Blue Ray film (VWR). The following antibodies were used for western blot analyses: rabbit
703 anti-Flag polyclonal (Sigma Aldrich), rabbit anti-PIAS1 polyclonal (Cell Signaling Technology), rabbit anti-
704 Myc polyclonal (Cell Signaling Technology), rabbit anti-His (Sigma Aldrich), rabbit anti-Tubulin polyclonal
705 antibody (Cell Signaling Technology).

706 ***Fluorescence imaging and co-localization analysis***

707 HEK-SUMO3m cells were plated on 12-mm-diameter coverslips until they reached the desired density
708 level and then transfected with the desired plasmids for 48 h. Cells were fixed in 4% paraformaldehyde
709 (in PBS) for 15 min, followed by a 2-min permeabilization with 0.1% Triton X-100 (in PBS) and saturation
710 with 2% BSA (in PBS) for 15 min. Cells were incubated with the primary antibodies for 1 h at 37 °C, rinsed
711 and incubated with secondary antibodies conjugated to Alexa Fluor (Cell Signaling Technology) and DAPI
712 (Sigma Aldrich) for 1 h at room temperature. Both primary and secondary antibodies are diluted in PBS /
713 BSA 2%. To reach sub-diffraction resolution, images from fixed samples were acquired with the Airyscan
714 detector of a Zeiss LSM880 confocal equipped with a 63X/1.43 Plan Apochromat oil immersion objective.
715 We automatically detected and assessed the number of PIAS1 and PML positive structures by using the
716 "particle analysis" tool from ImageJ. We then calculated the ratio manually.

717 ***In-gel Digestion and LC-MS/MS Identification***

718 Cell pellets were resuspended in 5 pellet volumes of ice cold RIPA buffer. The lysate was spun at 13 000 g
719 for 10 minutes to separate the extract into RIPA soluble and insoluble fractions. The soluble and insoluble

720 VIM samples were separated on a 4–12% SDS-PAGE (Bio-rad), and the proteins were visualized by
721 coomassie staining. The gel lane around vimentin corresponding position (57 kDa) was cut and then diced
722 into ~1 mm^3 cubes. During the process of in-gel digestion, the gel pieces were first destained completely
723 using destaining solution (50% H_2O, 40% methanol, and 10% acetic acid). Then the gel pieces were
724 dehydrated by washing several times in 50% acetonitrile (ACN) until the gel pieces shriveled and looked
725 completely white. The proteins were reduced in 10 mM DTT at 56 ^oC for 30 min, alkylated in 55 mM
726 iodoacetamide at room temperature (RT) in the dark for 30 min, and digested overnight with 300 ng of
727 sequencing grade modified trypsin in 50 mM ammonium bicarbonate . The supernatants were transferred
728 into Eppendorf tubes, and the gel pieces were sonicated twice in extraction buffer (67% ACN and 2.5%
729 trifluoroacetic acid). Finally, the peptide extraction and the initial digest solution supernatant were
730 combined and then dried using a Speed Vac. Peptides were reconstituted in water containing 0.2% formic
731 acid and analyzed by nanoflow-LC-MS/MS using an Orbitrap Q Exactive HF Mass spectrometer (Thermo
732 Fisher Scientific) as described previously[66].

733 ***Fluorescence Recovery After Photobleaching (FRAP) assay***

734 The FRAP assays were conducted on a LSM 880 confocal microscope equipped with a thermostatized
735 chamber at 37 °C. The Vimentin Emerald expressing cells were detected using a GaAsp detector. Bleaching
736 was done by combining "Time", "Bleach" and "Region" modes on Zen software from Zeiss. Briefly, 5 pre-
737 bleach images were taken every 5 seconds, after which five pulses of a 488 nm laser were applied to
738 bleach an area of 25 × 2 µm. Post-bleach images were acquired every 5 seconds for 5 minutes. For
739 fluorescence recovery analysis, the intensity in the bleached region was measured varying time points
740 with "Frap profiler" plugin in ImageJ software. Bleach data were normalized to unbleached regions for all
741 the time points and expressed in arbitrary units in the recovery graphs.

742 ***Quantification of Vimentin organization.***

743 Fixed images of cells expressing Emerald-VIM^{wt} or Emerald-VIM^{mt} were taken using a LSM 880 confocal
744 microscope. The "title" mode in the Zen software from Zeiss was used to cover a large area of cells
745 (2,13mm x 2,13mm). To avoid localization and conformation artefacts due to expression levels, only the
746 cells expressing Emerald-Vimentin at an intermediate level were evaluated using the threshold module in
747 ImageJ. The same manual threshold was used for all conditions. Cells were tabulated using the "Cell
748 counter" plugin in ImageJ into 4 categories: ULF, VIFs, cytosolic and total cells. Categories specification

749 were performed manually and subjectively. A representative image of each category is shown in Figure
750 S9. More than 250 cells were counted for each experiments (N=3, n total cells = 750).

751

752 ***Statistical Analysis***

753 Statistical analysis was carried out to assess differences between experimental groups. Statistical
754 significance was analyzed by the Student's t-tests. $p<0.05$ was considered to be statistically significant.
755 One asterisk and two asterisks indicate $p<0.05$ and $p<0.01$, respectively.

756

757 **References**

758 1 Flotho, A. & Melchior, F. in *Annual Review of Biochemistry, Vol 82* Vol. 82 *Annual Review*
759 *of Biochemistry* 357-385 (Annual Reviews, 2013).
760 2 Liang, Y. C. *et al.* SUMO5, a Novel Poly-SUMO Isoform, Regulates PML Nuclear Bodies.
761 *Scientific Reports* **6**, 15, doi:10.1038/srep26509 (2016).
762 3 Kunz, K., Piller, T. & Muller, S. SUMO-specific proteases and isopeptidases of the SENP
763 family at a glance. *J Cell Sci* **131**, doi:10.1242/jcs.211904 (2018).
764 4 Mukhopadhyay, D. & Dasso, M. Modification in reverse: the SUMO proteases. *Trends in*
765 *Biochemical Sciences* **32**, 286-295, doi:10.1016/j.tibs.2007.05.002 (2007).
766 5 Liu, B. & Shuai, K. Regulation of the sumoylation system in gene expression. *Current*
767 *Opinion in Cell Biology* **20**, 288-293, doi:10.1016/j.ceb.2008.03.014 (2008).
768 6 Sampson, D. A., Wang, M. & Matunis, M. J. The small ubiquitin-like modifier-1 (SUMO-1)
769 consensus sequence mediates Ubc9 binding and is essential for SURIO-1 modification.
770 *Journal of Biological Chemistry* **276**, 21664-21669, doi:10.1074/jbc.M100006200 (2001).
771 7 Johnson, E. S. Protein modification by SUMO. *Annual Review of Biochemistry* **73**, 355-382,
772 doi:10.1146/annurev.biochem.73.011303.074118 (2004).
773 8 Shuai, K. & Liu, B. Regulation of gene-activation pathways by pias proteins in the immune
774 system. *Nature Reviews Immunology* **5**, 593-605, doi:10.1038/nri1667 (2005).
775 9 Rytinki, M. M., Kaikkonen, S., Pehkonen, P., Jaaskelainen, T. & Palvimo, J. J. PIAS proteins:
776 pleiotropic interactors associated with SUMO. *Cellular and Molecular Life Sciences* **66**,
777 3029-3041, doi:10.1007/s00018-009-0061-z (2009).
778 10 Tan, J. A. T., Song, J., Chen, Y. & Durrin, L. K. Phosphorylation-Dependent Interaction of
779 SATB1 and PIAS1 Directs SUMO-Regulated Caspase Cleavage of SATB1. *Molecular and*
780 *Cellular Biology* **30**, 2823-2836, doi:10.1128/mcb.01603-09 (2010).
781 11 Okubo, S. *et al.* NMR structure of the N-terminal domain of SUMO ligase PIAS1 and its
782 interaction with tumor suppressor p53 and A/T-rich DNA oligomers. *Journal of Biological*
783 *Chemistry* **279**, 31455-31461, doi:10.1074/jbc.M403561200 (2004).
784 12 Kipp, M. *et al.* SAF-Box, a conserved protein domain that specifically recognizes scaffold
785 attachment region DNA. *Molecular and Cellular Biology* **20**, 7480-7489,
786 doi:10.1128/mcb.20.20.7480-7489.2000 (2000).
787 13 van den Akker, E. *et al.* FLI-1 functionally interacts with PIASx alpha, a member of the PIAS
788 E3 SUMO ligase family. *Journal of Biological Chemistry* **280**, 38035-38046,
789 doi:10.1074/jbc.M502938200 (2005).
790 14 Duval, D., Duval, G., Kedinger, C., Poch, O. & Boeuf, H. The 'PINIT' motif, of a newly
791 identified conserved domain of the PIAS protein family, is essential for nuclear retention
792 of PIAS3L. *FEBS Lett.* **554**, 111-118, doi:10.1016/s0014-5793(03)01116-5 (2003).
793 15 Palvimo, J. J. PIAS proteins as regulators of small ubiquitin-related modifier (SUMO)
794 modifications and transcription. *Biochemical Society Transactions* **35**, 1405-1408,
795 doi:10.1042/bst0351405 (2007).
796 16 Kahyo, T., Nishida, T. & Yasuda, H. Involvement of PIAS1 in the sumoylation of tumor
797 suppressor p53. *Molecular Cell* **8**, 713-718, doi:10.1016/s1097-2765(01)00349-5 (2001).
798 17 Gross, M. *et al.* Distinct effects of PIAS proteins on androgen-mediated gene activation in
799 prostate cancer cells. *Oncogene* **20**, 3880-3887, doi:10.1038/sj.onc.1204489 (2001).

800 18 Megidish, T., Xu, J. H. & Xu, C. W. Activation of p53 by protein inhibitor of activated Stat1
801 (PIAS1). *Journal of Biological Chemistry* **277**, 8255-8259, doi:10.1074/jbc.C2000001200
802 (2002).
803 19 Liu, B. *et al.* Inhibition of Stat1-mediated gene activation by PIAS1. *Proceedings of the*
804 *National Academy of Sciences of the United States of America* **95**, 10626-10631,
805 doi:10.1073/pnas.95.18.10626 (1998).
806 20 Driscoll, J. J. *et al.* The sumoylation pathway is dysregulated in multiple myeloma and is
807 associated with adverse patient outcome. *Blood* **115**, 2827-2834, doi:10.1182/blood-
808 2009-03-211045 (2010).
809 21 Hoefer, J. *et al.* PIAS1 Is Increased in Human Prostate Cancer and Enhances Proliferation
810 through Inhibition of p21. *American Journal of Pathology* **180**, 2097-2107,
811 doi:10.1016/j.ajpath.2012.01.026 (2012).
812 22 Puhr, M. *et al.* PIAS1 is a determinant of poor survival and acts as a positive feedback
813 regulator of AR signaling through enhanced AR stabilization in prostate cancer. *Oncogene*
814 **35**, 2322-2332, doi:10.1038/onc.2015.292 (2016).
815 23 Rabellino, A. *et al.* PIAS1 Promotes Lymphomagenesis through MYC Upregulation. *Cell*
816 *Reports* **15**, 2266-2278, doi:10.1016/j.celrep.2016.05.015 (2016).
817 24 Kadare, G. *et al.* PIAS1-mediated sumoylation of focal adhesion kinase activates its
818 autophosphorylation. *Journal of Biological Chemistry* **278**, 47434-47440,
819 doi:10.1074/jbc.M308562200 (2003).
820 25 Streich, F. C. & Lima, C. D. Capturing a substrate in an activated RING E3/E2-SUMO
821 complex. *Nature* **536**, 304-+, doi:10.1038/nature19071 (2016).
822 26 Rabellino, A. *et al.* The SUMO E3-ligase PIAS1 Regulates the Tumor Suppressor PML and
823 Its Oncogenic Counterpart PML-RARA. *Cancer Res.* **72**, 2275-2284, doi:10.1158/0008-
824 5472.can-11-3159 (2012).
825 27 Lamoliatte, F., McManus, F. P., Maarifi, G., Chelbi-Alix, M. K. & Thibault, P. Uncovering the
826 SUMOylation and ubiquitylation crosstalk in human cells using sequential peptide
827 immunopurification. *Nature Communications* **8**, 11, doi:10.1038/ncomms14109 (2017).
828 28 Hendriks, I. A. *et al.* Uncovering global SUMOylation signaling networks in a site-specific
829 manner. *Nature Structural & Molecular Biology* **21**, 927-936, doi:10.1038/nsmb.2890
830 (2014).
831 29 Snider, N. T., Weerasinghe, S. V., Iniguez-Lluhi, J. A., Herrmann, H. & Omary, M. B. Keratin
832 hypersumoylation alters filament dynamics and is a marker for human liver disease and
833 keratin mutation. *J Biol Chem* **286**, 2273-2284, doi:10.1074/jbc.M110.171314 (2011).
834 30 Goodman, S. R. *Medical cell biology*. (Academic Press, 2007).
835 31 Hochstrasser, M. SP-RING for SUMO: new functions bloom for a ubiquitin-like protein.
836 *Cell* **107**, 5-8 (2001).
837 32 Brown, J. R. *et al.* SUMO Ligase Protein Inhibitor of Activated STAT1 (PIAS1) Is a
838 Constituent Promyelocytic Leukemia Nuclear Body Protein That Contributes to the
839 Intrinsic Antiviral Immune Response to Herpes Simplex Virus 1. *Journal of Virology* **90**,
840 5939-5952, doi:10.1128/jvi.00426-16 (2016).
841 33 Lane, E. B., Hogan, B. L. M., Kurkinen, M. & Garrels, J. I. CO-EXPRESSION OF VIMENTIN
842 AND CYTOKERATINS IN PARIETAL ENDODERM CELLS OF EARLY MOUSE EMBRYO. *Nature*
843 **303**, 701-704, doi:10.1038/303701a0 (1983).

844 34 Ramaekers, F. C. S. *et al.* COEXPRESSION OF KERATIN-TYPE AND VIMENTIN-TYPE
845 INTERMEDIATE FILAMENTS IN HUMAN METASTATIC CARCINOMA-CELLS. *Proceedings of*
846 *the National Academy of Sciences of the United States of America-Biological Sciences* **80**,
847 2618-2622, doi:10.1073/pnas.80.9.2618 (1983).
848 35 Thomas, J. T., Hubert, W. G., Ruesch, M. N. & Laimins, L. A. Human papillomavirus type 31
849 oncoproteins E6 and E7 are required for the maintenance of episomes during the viral life
850 cycle in normal human keratinocytes. *Proceedings of the National Academy of Sciences of*
851 *the United States of America* **96**, 8449-8454, doi:10.1073/pnas.96.15.8449 (1999).
852 36 Anastasi, E. *et al.* Expression of Reg and cytokeratin 20 during ductal cell differentiation
853 and proliferation in a mouse model of autoimmune diabetes. *European Journal of*
854 *Endocrinology* **141**, 644-652, doi:10.1530/eje.0.1410644 (1999).
855 37 Chu, Y. W., Runyan, R. B., Oshima, R. G. & Hendrix, M. J. C. EXPRESSION OF COMPLETE
856 KERATIN FILAMENTS IN MOUSE L-CELLS AUGMENTS CELL-MIGRATION AND INVASION.
857 *Proceedings of the National Academy of Sciences of the United States of America* **90**, 4261-
858 4265, doi:10.1073/pnas.90.9.4261 (1993).
859 38 Bordeleau, F., Bessard, J., Sheng, Y. & Marceau, N. Keratin contribution to cellular
860 mechanical stress response at focal adhesions as assayed by laser tweezers. *Biochemistry*
861 *and Cell Biology-Biochimie Et Biologie Cellulaire* **86**, 352-359, doi:10.1139/o08-076 (2008).
862 39 Hu, G., Jia, F., Gao, N. & Han, Y. Impacts of CyhospitalclinE downstream vimentin on
863 proliferation, invasion and apoptosis of hepatoma HepG2 cell. *International Journal of*
864 *Clinical and Experimental Medicine* **11**, 5564-5571 (2018).
865 40 Snider, N. T. & Omary, M. B. Post-translational modifications of intermediate filament
866 proteins: mechanisms and functions. *Nature Reviews Molecular Cell Biology* **15**, 163-177,
867 doi:10.1038/nrm3753 (2014).
868 41 Zhu, Q. S. *et al.* Vimentin is a novel AKT1 target mediating motility and invasion. *Oncogene*
869 **30**, 457-470, doi:10.1038/onc.2010.421 (2011).
870 42 Snider, N. T., Weerasinghe, S. V. W., Iniguez-Lluhi, J. A., Herrmann, H. & Omary, M. B.
871 Keratin Hypersumoylation Alters Filament Dynamics and Is a Marker for Human Liver
872 Disease and Keratin Mutation. *Journal of Biological Chemistry* **286**, 2273-2284,
873 doi:10.1074/jbc.M110.171314 (2011).
874 43 Goldman, R. D., Cleland, M. M., Murthy, S. N. P., Mahammad, S. & Kuczmarski, E. R.
875 Inroads into the structure and function of intermediate filament networks. *Journal of*
876 *Structural Biology* **177**, 14-23, doi:10.1016/j.jsb.2011.11.017 (2012).
877 44 Helfand, B. T. *et al.* Vimentin organization modulates the formation of lamellipodia.
878 *Molecular Biology of the Cell* **22**, 1274-1289, doi:10.1091/mbc.E10-08-0699 (2011).
879 45 Perez-Sala, D. *et al.* Vimentin filament organization and stress sensing depend on its single
880 cysteine residue and zinc binding. *Nature Communications* **6**, doi:10.1038/ncomms8287
881 (2015).
882 46 Satelli, A. & Li, S. L. Vimentin in cancer and its potential as a molecular target for cancer
883 therapy. *Cellular and Molecular Life Sciences* **68**, 3033-3046, doi:10.1007/s00018-011-
884 0735-1 (2011).
885 47 Eriksson, J. E. *et al.* Specific in vivo phosphorylation sites determine the assembly
886 dynamics of vimentin intermediate filaments. *Journal of Cell Science* **117**, 919-932,
887 doi:10.1242/jcs.00906 (2004).

888 48 Robert, A., Rossow, M. J., Hookway, C., Adam, S. A. & Gelfand, V. I. Vimentin filament
889 precursors exchange subunits in an ATP-dependent manner. *Proc. Natl. Acad. Sci. U. S. A.*
890 **112**, E3505-E3514, doi:10.1073/pnas.1505303112 (2015).
891 49 Premchandar, A. *et al.* Structural Dynamics of the Vimentin Coiled-coil Contact Regions
892 Involved in Filament Assembly as Revealed by Hydrogen-Deuterium Exchange. *Journal of*
893 *Biological Chemistry* **291**, 24931-24950, doi:10.1074/jbc.M116.748145 (2016).
894 50 Chou, Y. H., Khuon, S., Herrmann, H. & Goldman, R. D. Nestin promotes the
895 phosphorylation-dependent disassembly of vimentin intermediate filaments during
896 mitosis. *Molecular Biology of the Cell* **14**, 1468-1478, doi:10.1091/mbc.E02-08-0545
897 (2003).
898 51 Chen, P. *et al.* Protein inhibitor of activated STAT-1 is downregulated in gastric cancer
899 tissue and involved in cell metastasis. *Oncology Reports* **28**, 2149-2155,
900 doi:10.3892/or.2012.2030 (2012).
901 52 Suman, P. *et al.* AP-1 Transcription Factors, Mucin-Type Molecules and MMPs Regulate
902 the IL-11 Mediated Invasiveness of JEG-3 and HTR-8/SVneo Trophoblastic Cells. *Plos One*
903 **7**, 12, doi:10.1371/journal.pone.0029745 (2012).
904 53 Cuijpers, S. A. G., Willemstein, E. & Vertegaal, A. C. O. Converging Small Ubiquitin-like
905 Modifier (SUMO) and Ubiquitin Signaling: Improved Methodology Identifies Co-modified
906 Target Proteins. *Molecular & Cellular Proteomics* **16**, 2281-2295,
907 doi:10.1074/mcp.TIR117.000152 (2017).
908 54 Kumar, R., Gonzalez-Prieto, R., Xiao, Z. Y., Verlaan-de Vries, M. & Vertegaal, A. C. O. The
909 STUbL RNF4 regulates protein group SUMOylation by targeting the SUMO conjugation
910 machinery. *Nature Communications* **8**, doi:10.1038/s41467-017-01900-x (2017).
911 55 Cox, J. & Mann, M. MaxQuant enables high peptide identification rates, individualized
912 p.p.b.-range mass accuracies and proteome-wide protein quantification. *Nature*
913 *Biotechnology* **26**, 1367-1372, doi:10.1038/nbt.1511 (2008).
914 56 Cox, J. *et al.* Andromeda: A Peptide Search Engine Integrated into the MaxQuant
915 Environment. *Journal of Proteome Research* **10**, 1794-1805, doi:10.1021/pr101065j
916 (2011).
917 57 Feuermann, M., Gaudet, P., Mi, H. Y., Lewis, S. E. & Thomas, P. D. Large-scale inference of
918 gene function through phylogenetic annotation of Gene Ontology terms: case study of
919 the apoptosis and autophagy cellular processes. *Database-the Journal of Biological*
920 *Databases and Curation*, 11, doi:10.1093/database/baw155 (2016).
921 58 Mi, H. Y. *et al.* PANTHER version 11: expanded annotation data from Gene Ontology and
922 Reactome pathways, and data analysis tool enhancements. *Nucleic Acids Research* **45**,
923 D183-D189, doi:10.1093/nar/gkw1138 (2017).
924 59 Huang, D. W., Sherman, B. T. & Lempicki, R. A. Bioinformatics enrichment tools: paths
925 toward the comprehensive functional analysis of large gene lists. *Nucleic Acids Research*
926 **37**, 1-13, doi:10.1093/nar/gkn923 (2009).
927 60 Colaert, N., Helsens, K., Martens, L., Vandekerckhove, J. & Gevaert, K. Improved
928 visualization of protein consensus sequences by iceLogo. *Nature Methods* **6**, 786-787,
929 doi:10.1038/nmeth1109-786 (2009).

930 61 Petersen, B., Petersen, T. N., Andersen, P., Nielsen, M. & Lundegaard, C. A generic method
931 for assignment of reliability scores applied to solvent accessibility predictions. *Bmc*
932 *Structural Biology* **9**, 10, doi:10.1186/1472-6807-9-51 (2009).
933 62 von Mering, C. *et al.* STRING: a database of predicted functional associations between
934 proteins. *Nucleic Acids Research* **31**, 258-261, doi:10.1093/nar/gkg034 (2003).
935 63 Szklarczyk, D. *et al.* The STRING database in 2011: functional interaction networks of
936 proteins, globally integrated and scored. *Nucleic Acids Research* **39**, D561-D568,
937 doi:10.1093/nar/gkq973 (2011).
938 64 Shannon, P. *et al.* Cytoscape: A software environment for integrated models of
939 biomolecular interaction networks. *Genome Research* **13**, 2498-2504,
940 doi:10.1101/gr.1239303 (2003).
941 65 Cline, M. S. *et al.* Integration of biological networks and gene expression data using
942 Cytoscape. *Nature Protocols* **2**, 2366-2382, doi:10.1038/nprot.2007.324 (2007).
943 66 McManus, F. P., Lamoliatte, F. & Thibault, P. Identification of cross talk between
944 SUMOylation and ubiquitylation using a sequential peptide immunopurification
945 approach. *Nature protocols* **12**, 2342-2358, doi:10.1038/nprot.2017.105 (2017).

946